Insights in the chemical fundamentals of ASR and the role of calcium in the early stage based on a 3D reactive transport model

Qiu, Xiujiao; Chen, Jiayi; Ye, Guang; De Schutter, Geert

Important note
To cite this publication, please use the final published version (if applicable).
Please check the document version above.

Insights in the chemical fundamentals of ASR and the role of calcium in the early stage based on a 3D reactive transport model

Xiujiao Qiu [a],[1], Jiayi Chen [b],[1], Guang Ye [b], Geert De Schutter [a],[*]

[a] Department of Structural Engineering and Building Materials, Ghent University, Ghent 9052, Belgium
[b] Department of Materials, Mechanics, Management & Design, Delft University of Technology, Delft, 2600, AA, the Netherlands

ABSTRACT

Prediction of alkali silica reaction is still difficult due to the lack of a comprehensive understanding of its chemical fundamentals. In-site experimentally revealing the fundamentals is not realistic as ASR shows over several years or even decades and is affected by many factors. In this paper, by utilizing a 3D reactive-transport simulation model at microscale, we have numerically explored the fundamentals of ASR in the early stage under the influence of reactive silica fraction, alkali concentration, silica disorder degree and aggregate porosity. Based on the simulation results, the chemical sequences of ASR, the initial location of ASR products, the mechanism behind and the role of calcium under the influence of the above factors are elaborated. Furthermore, a comprehensive mechanism to explain the pessimum reactive aggregate content is derived. The results of this paper give some insights about ASR in the early stage such as the initial expansion locations.

1. Introduction

As one of the most severe durability issues in concrete, alkali silica reaction (ASR) has obtained significant attention since 1980s. The reaction happens between the pore solution in the cement paste and the reactive silica in the aggregate. The reaction products are able to induce expansive stress that is able to crack the surrounding materials and even the whole structure. Numerous studies have been conducted to understand and predict this deleterious reaction [1]. Unfortunately, the fundamental mechanisms of ASR are still not very clear and predicting ASR is still difficult.

One of the the main challenges to predict ASR is that it is such a complicated process influenced by many factors including but not limited to aggregate mineralogy, reactive aggregate content, aggregate size, aggregate porosity, alkali concentration in the pore solution, moisture, presence of calcium [1–3] and temperature. The same rock originating from different geological environment may behave totally different depending on the silica polymorphs contained by the rock. Amorphous silica shows a much higher destructive ability than the crystal silica. On the other hand, a pessimum reactive silica content and a pessimum size have been found for some reactive aggregate such as opal. The ASR induced concrete expansion with these reactive

aggregates increases with the increasing aggregate content or aggregate size until reaches it maximum value at the pessimum content or pessimum size. With the aggregate content or size further increasing, the expansion decreases [4–7]. The pessimum content and pessimum size vary a lot among the aggregate type. For the highly reactive aggregate, such as opal and chert, maximum expansion occurs for low content (usually below 10%) of reactive silica [8,9]. Nevertheless, for slowly reactive aggregates, the pessimum content is much higher, even up to 100% which means there is no pessimum effect. Obviously, the pessimum reactive silica content decreases as the silica reactivity increases. But for the pessimum aggregate size, there is no general pattern [1]. The mechanisms proposed to explain these pessimum phenomenon are not all in agreement as will be discussed in Section 4.2. Furthermore, it has also been reported that increased aggregate porosity may enhance the alkali reactivity, due to easier access for ions from the concrete pore solution [10].

Except for the reactive aggregate, it is agreed in literature that there are two more basic conditions needed for ASR [2,11]: a high alkali concentration and sufficient moisture. Based on Santon's [12] early work, it was proposed that an upper limit of the alkali concentration of the cement is around 0.5 mol L^{-1} when the water/cement ratio is 0.5 (0.6% Na_2O_e by mass of cement) to avoid ASR. However, different

---

threshold alkali concentrations under different conditions for ASR have been continuously reported in literature. A value of 0.22 mol L^{-1} was suggested proposed by Diamond [13,14], while a value of 0.65 mol L^{-1} was reported by Multon et al. [15] and Gao et al. [16]. This indicates that the influential mechanism of alkali concentration on ASR is still not fully understood and limiting the alkali content of cement is not always an effective way to prevent ASR in structures with different reactive aggregates used or under different conditions. Nevertheless, a general pattern is that the reaction rate of ASR increases as the alkali concentration increases [14].

For the influence of moisture, it is widely agreed in literature that sufficient moisture is required for ASR expansion [17]. When the internal relative humidity (RH) inside the concrete falls below a threshold value, ASR stops. The threshold RH value is found to depend on temperature that it decreases as temperature increasing. The value drops from 80% to 50% when the temperature increases from 20 °C [18] to 60 °C [19].

Calcium plays an important role in the formation of ASR reaction products as it controls aggregation and gelation processes in silicoalkaline solutions [20,21]. However, the influence of calcium on expansion due to ASR is not consistent. Some studies show that the presence of calcium in ASR products decreases its expansion capability [22], while some conclude that the presence of calcium is a prerequisite for ASR expansion [23–25]. The last influencing factor, temperature, is able to faster dissolve the silica thus increasing the expansion [26].

Another challenge is that it is difficult to capture the chemical process experimentally in field in a long term because ASR usually happens over several years or decades [2]. Accelerated testing methods are normally adopted in the laboratory to evaluate ASR by increasing temperature and alkali concentration. Nevertheless, as concluded by Lindgård [27], none of the existing testing methods have proven to be reliable for use with all aggregate types. Further more, there is a risk that the mechanism could be changed by the acceleration techniques. An alternative approach to fulfill this goal is through numerical simulation. In our previous paper [28], we have proposed a 3D reactive transport model for simulating the chemical reaction process of ASR at microscale in the early stage including the dissolution of silica, the nucleation and growth of ASR product surrogates and the dissolution of calcium hydroxide (CH) and calcium silicate hydrate (C-S-H). The results showed that the proposed model is able to capture the chemical sequences of ASR and to simulate the typical location patterns of ASR products as found in experiments and in field concrete. Based on this model, it is possible to have a deep exploration of the chemical fundamentals of ASR in the early stage under different influential factors.

In this paper, we utilized the model [28] to simulate the chemical process of ASR under four representative significant influential factors: reactive silica content in aggregate, alkali concentration, silica microstructural disorder degree and aggregate porosity. The size of aggregate is not considered based on the fact that our model focus at microscale. The temperature is set to 25 °C in the model based on the fact that the thermodynamic data of the chemical reactions (see Section 2.1) involved in the model are usually obtained at this temperature. The internal RH is set to 100% to exclude its influence.

The aim of the paper is to investigate the chemical fundamental mechanism of the ASR process in the early stage under a single or coupled influence of different factors. The influence of the above factors on the chemical reaction sequence, the location of the produced products are investigated. It has been shown in literature that the presence of CH is a necessary condition for ASR as it acts as a "buffer" providing extra Ca^{2+} and OH^- for ASR [24,29]. Recently, thermodynamic simulation also showed that C-S-H in the cement paste can be a Ca^{2+} and OH^- buffer too [30]. Thus, the role of calcium is also studied by considering the dissolution of CH and C-S-H in the model. The influence of the above factors on the CH and C-S-H dissolution is also clarified. The paper firstly introduces the former proposed model briefly. Then, the parameter settings for the simulations used in this paper are outlined. After that,

the simulation results are explained and discussed.

2. Methods

2.1. A 3D reactive transport model

As stated before, a 3D reactive transport model is developed to simulate the fundamental mechanism of ASR at microscale in the early stage. A brief introduction about the model is firstly stated below.

The model simulates ASR in a 3D domain of interest composed of a representative cement paste microstructure including the interfacial transition zone (ITZ) with a size of $100 \times 100 \times 100 \ \mu m^3$ and aggregate microstructure with a size of $100 \times 100 \times 100 \ \mu m^3$ as shown in Fig. 1. Both of the microstructures are obtained through numerical simulation. The microstructure of the cement paste with an initial water/cement (w/c) ratio of 0.4 is simulated at a hydration degree of 78% using a cement hydration simulation model of Chen and Ye extended from [31]. The final simulated microstructure is mainly composed of unhydrated cements, saturated pores, CH, C1.1SH3.9, C1.5SH2, AFm as shown in the 2D slice of Fig. 1. The pore solution ions diffuse through these hydration products with different diffusion coefficients to the aggregate to trigger ASR. C1.1SH3.9, C1.5SH2 and CH are supposed to dissolve, as a response to the local thermodynamic state change due to ASR, to buffer the calcium and hydroxide ions. The size of ITZ in the microstructure is around 10 μm. The microstructure of an aggregate, a siliceous limestone with the alkali silica reactivity attributing to cryptocrystalline and microcrystalline silica (the only silica form in the stone), is simulated from 2D scanning electron microscope-backscattered (SEM-BSE) images using the autocorrelation function. For this part of work, one can refer to [32]. Limited by the computer capacity, the pores below a size of 1 μm are lost and the final microstructure is composed of air voids, reactive silica and other nonreactive minerals. Due to the heterogeneity of the aggregate, five 3D microstructures (represented by microstructure 1 to microstructure 5) with a size of $100 \times 100 \times 100 \ \mu m^3$ are obtained. In each cube, the size and fraction of the reactive silica as well as the pore are different. The fraction of the reactive silica in each microstructure is shown in the second column in Table 3.

Fig. 2 shows six random slices of reactive silica distribution from the simulated 3D microstructure 1 with the lowest reactive silica fraction of 6.58% and from microstructure 5 with the highest reactive silica fraction of 40.91% and their original binarized SEM-BSE images. Fig. 2a shows that at a lower reactive silica fraction, the reactive silica particle sizes are smaller and distributed sparsely in the simulated model, which is similar to the original image. For a higher reactive silica fraction in Fig. 2b, reactive silica particles are clustered together which makes the structure more closely connected. This characteristic is also simulated relatively successfully if one compares it with the original one. Furthermore, the simulated particle size distribution of the reactive silica particles and air voids are also consistent to the original one. Further explanation can be found in [32].

The simulated ions in the pore solution of cement paste are $Al(OH)_4^-$, $Fe(OH)_4^-$, SO_4^{2-}, Ca^{2+}, OH^-, Na^+, K^+, $H_2SiO_4^{2-}$. Only the last five ions are related to ASR. Thus in the model, only the last five ions are considered. These ions are able to diffuse within the pore, low density C1.1SH3.9, high density C1.5SH2, ASR products (KSH and TobH explained below) and all the phases in the aggregate with different diffusion coefficients in different phases, while the other crystal phases such as AFm and CH, are impermeable. The diffusion coefficients are listed in Table 1. The anisotropic diffusion is simulated using the multi-relaxation time (MRT) lattice Boltzmann method instead of the most popular Bathnagar-Gross-Krook (BGK) method [34]. The MRT model provides the advantage over BGK that the influence of the relaxation time τ on the ion diffusion is greatly decreased so that a relatively large τ (1200 in this work) can be adopted to decrease the number of iterations while not sacrificing the ion diffusion accuracy [35], especially for the
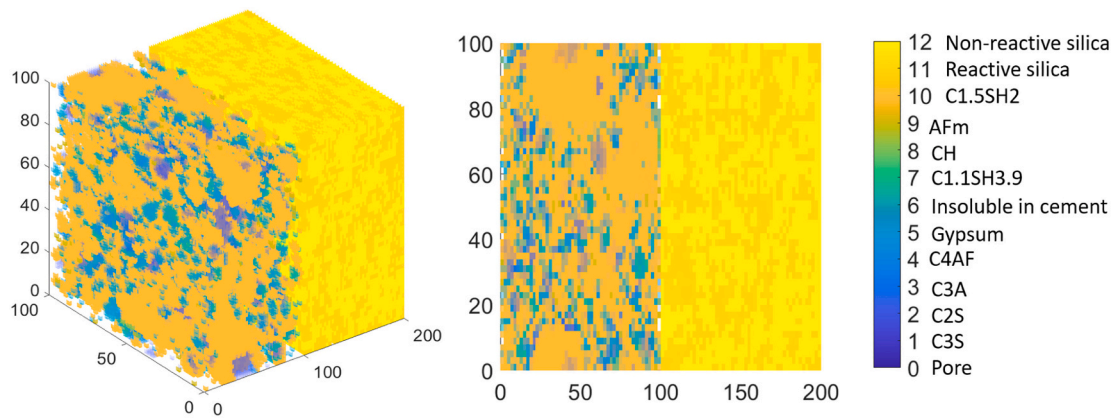
Fig. 1. A schematic diagram of the 3D domain of interest in the model and a 2D slice from the 3D domain. The left cube is cement paste and the right cube is aggregate. Different color represents different phases. unit of scale: μm.
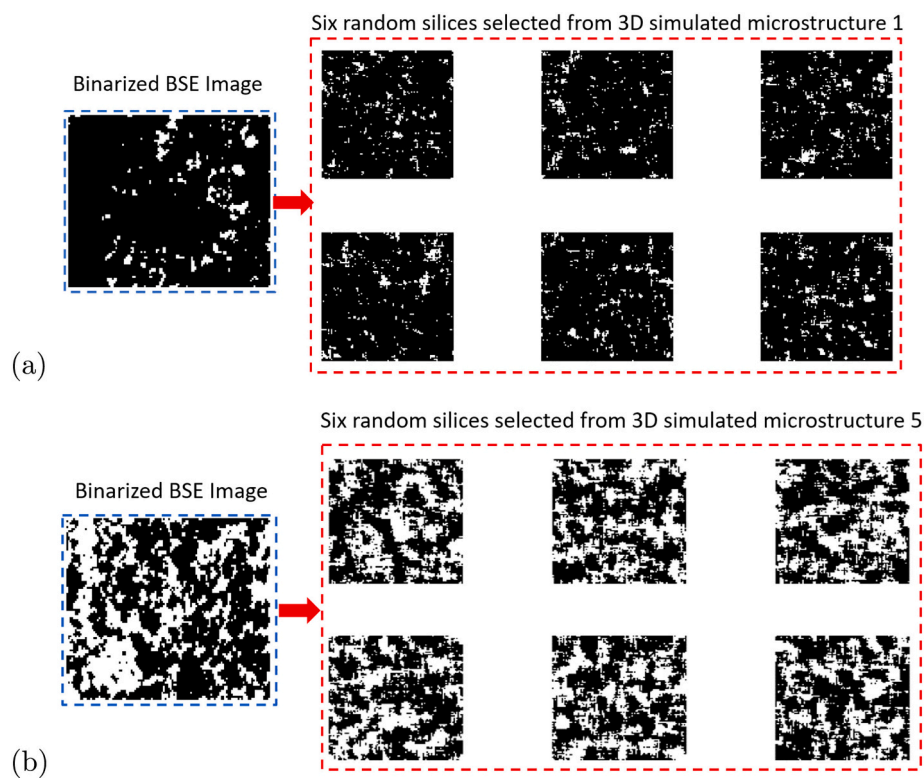

Fig. 2. Two examples of 2D original and simulated quartz distribution. (**a**): Comparison between six 2D sections from the simulated microstructure 1 with 6.58% quartz fraction and the original 2D binarized image; (**b**): Comparison between the 2D sections from the simulated microstructure 5 with 40.91% quartz fraction and the original 2D binarized image. White:quartz; Black: pore and the others.

Table 1
Diffusion coefficients of ASR related ions in different phases.

Phase	Diffusion coefficients, m^2/s
Pore (D_w)	$[0.72(Ca^{2+}), 5.30(OH^-), 1.33(Na^+), 1.80(K^+), 0.70 (H_2SiO_4{}^{2-})] \times 10^{-9}$ [33]
Low density C1.1SH3.9 (D_{LD})	$\frac{1}{80}D_w$ [31]
High density C1.5SH2 (D_{HD})	$\frac{1}{720}D_w$ [31]
Low Ca/Si ASR product (D_{KSH})	$\frac{1}{80}D_w$
High Ca/Si ASR product (D_{TobH})	$\frac{1}{720}D_w$
Aggregate (D_{agg})	$4 \times 10^{-7}D_w$ [28]

case in which the diffusion coefficients vary spatially. This method requires only seven velocities in three dimensions. The method is not elaborated here due to the space limitation. More details can be found in [36].

Alkalis have different interactions with the reactive silica in the ASR system. It was reported that the silica's interaction with K^+ has a higher dissolution rate (around 1.3 times) than that with Na^+ [37]. The formation of ASR products is a process of condensation and polymerization of the dissolved silica. In the high alkaline solution in concrete, most of the dissolved silica ions are $H_2SiO_4{}^{2-}$. Without the help of alkalis, condensation can happen but is very limited due to the electrostatic repulsive forces between the charged silica ions. The alkalis are able to form a shielding double layer around each silica particle, which reduces the electrostatic repulsive forces and leads to condensation of ASR

products. It is also found that K^+ has a higher shielding capability than Na^+ due to less strongly bound water, which means less K^+ is needed than Na^+ to condensate a same amount of dissolved silica [38]. But they behave kinetically similarly during the gelation as reported in [39]. Furthermore, the chemical compositions of formed Na-ASR products and K-ASR products are also similar to each other as found in [40]. Based on these findings and the fact that most of the alkalis in the pore solution of concrete are K^+ (1.3 wt% of K_2SiO_4 and 0.3 wt% wt of Na^+ in the cement used in this work), Na^+ is transferred to an equivalent mass of K^+ in the model. This causes a discrepancy of the silica dissolution rate. But the difference would not cause much influence on ASR since compared with the alkali type, the dissolution rate of the reactive silica is mainly affected by the OH^-, the temperature and the reactivity of the silica itself.

The chemical reactions involved in ASR are thermodynamic-kinetically simulated inside the domain coupled with the ions diffusion. The reactions include: (a) dissolution of silica in the aggregate; (b) dissolution of CH in the cement paste; (c) dissolution of C-S-H in the cement paste; (d) formation of ASR product surrogates. In 2019 Leemann et al. [41] have investigated the reaction sequence of ASR by adding caesium to concrete. The results implicated that it is the formation of the amorphous ASR products that cause the initial expansion of the structure. They have also characterized the chemical compositional difference of the amorphous and the mature crystalline ASR products formed in concrete by using Raman microscopy [42]. The average Ca/Si ratio and alkali/Si ratio of these two products are very similar with values of 0.21–0.23 and 0.22–0.26, while the main difference concerns the Na/K ratio with higher values in the amorphous products compared to the crystalline ones. The discovered Ca/Si and Alkali/Si ratio are similar to the synthesized crystal product K-shlykovite in the work of Shi et al. [40], which is identical to that formed in field concrete. Therefore, in this work, surrogate K-shlykovite ($KCaSi_4O_8(OH)_3 \cdot 2.9H_2O$, KSH) is selected to represent the amorphous ASR products accounting for the initial cracking. Besides, tobermorite ($(CaO)_{0.6667}SiO_2(OH)_3 \cdot 1.5H_2O$, abbreviated as TobH) is also considered since it was also observed in the synthesis experimental researches of [39,40,43]. The chemical reaction formulas and adopted thermodynamic equilibrium constants are shown in Table 2. Except the equilibrium constant of KSH formation, all other equilibrium constants are collected from [44]. The equilibrium constant of KSH formation is obtained through sensitivity analysis which is stated in [28] due to lacking data in literature. The equilibrium constant of silica dissolution is the solubility of crystal silica in water. With pH increasing, due to the ionization effect, the solubility of silica will increase. When the pH increases from 7 to 14, the solubility of amorphous silica increases from 1×10^{-3} to 1×10^2 mol $\cdot$ L^{-1} [1]. Thus, the solubility of silica is adjusted in the model according to the local pH. Obviously, with such a high solubility in alkaline solution, the pore solution in concrete will keep undersaturated for silica dissolution.

The dissolution kinetics of the above reactions plus the nucleation and growth kinetics of TobH and KSH are implemented in the model. More details can be found in the previous paper [28]. In the model, as the local solution near to silica nodes or CH nodes or C-S-H nodes is undersaturated for dissolution, they will start to dissolve. The dissolved ions then are diffused out from the dissolution sites to other locations for

further reactions. Due to the lack of the kinetic information about the nucleation and growth of the ASR products, the classical nucleation and growth theory is adopted in the model. According to the theory, ASR products begin to nucleate when the local solution reaches a thermodynamic supersaturation state. The location of the nuclei of ASR products in the domain is simulated based on the probability distribution theory that at a constant supersaturation degree, the appearance of a nuclei can be regarded as a random process and as independent and can be described by the Poisson distribution [45].

Three types of nodes are available for ASR products to nucleate and grow in the simulation domain. Type 1 is the pore nodes. Type 2 is the partially empty nodes in the cement paste and type 3 is the partially dissolved silica nodes in the aggregate. During the simulation, the saturation degree of these non-full nodes for KSH and TobH are firstly calculated. The supersaturated nodes (saturation degree larger than 1) are then extracted for ASR products to nucleate and grow. When a node is fully filled, then it is able to redistribute its extra mass of ASR products to its adjacent empty or partially empty nodes. If there is no empty place around, the extra ASR products are accumulated in the full nodes. Expansion is then caused. What should be noticed here is that the extra mass is only induced by KSH. This is because KSH has a large expansion ratio (the volume of a given amount of KSH to the volume of the same amount of the reactive silica), which means its density is very small compared to the reactive silica (2500 kg $\cdot$ m^{-3} for the reactive silica in the model). The study of [40,46] have shown that the synthesized shlykovite-like crystalline ASR products have a solid density more than 2200 kg $\cdot$ m^{-3}. However, the products are observed to be very porous, which is possible to result in a much smaller bulk density. A fitting expansion ratio value of 0.5 is also found in [47] and is used in this work. The expansion ratio of TobH (density of around 2500 kg $\cdot$ m^{-3}) is very small or even smaller than zero depending on the silica density. However, the C-S-H can act as a barrier to accumulate the extra KSH. When a KSH node is surrounded by TobH, the ions can diffuse through it but the formed KSH cannot diffuse out of it.

2.2. Simulations

Based on the model, simulations were done to investigate the influence of reactive silica content in aggregate, alkali concentration, silica microstructural disorder degree and aggregate porosity on ASR.

The influence of reactive silica content in aggregate was realized by changing the aggregate microstructure. As stated before, we have obtained five different microstructures to represent the reactive limestone. Each microstructure contains a different fractions and distributions of silica and air void (reactive silica content varies from 6.58% to 40.91%, air void fraction varies from 0.11% to 2.77%). In this paper, these five microstructures were inputted into the model to investigate the influence of reactive silica content in aggregate on ASR. The simulations are referred to the system S series as shown in Table 3 in the continuation of the paper.

The influence of alkali concentration was realized by changing the initial alkali concentration in the cement paste. Alkali concentration of cement paste is the results of clinker composition, w/c ratio, and degree of hydration reaction. The average equivalent K_{eq}^+ concentration in the simulated cement paste, with 0.35% Na_2Oe by mass of cement contained

Table 2
The determined equilibrium constant for thermodynamic simulations.

	Chemical reaction formula	Equilibrium constant
Silica dissolution	$SiO_{2(s)} + 2OH^- \rightarrow H_2SiO_4^{2-}$	$\log K_1 = -3.73$
CH dissolution	$Ca(OH)_2 \rightarrow Ca^{2+} + 2OH^-$	$\log K_2 = -5.2$
C-S-H Dissolution	$Ca_{1.1}SiO2(OH)_{2.2} \cdot 2.8H_2O \rightarrow 1.1Ca^{2+} + H_2SiO_4^{2-} + 0.2OH^- + 2.8H_2O$	$\log K_3 = -7.85$
	$(CaO)_{1.5}SiO_2 \cdot 2H_2O \rightarrow 1.5Ca^{2+} + H_2SiO_4^{2-} + OH^- + 0.5H_2O$	$\log K_4 = -11.46$
KSH formation	$Ca^{2+} + K^+ + 4H_2SiO_4^{2-} + 2.9H_2O \rightarrow KCaSi_4O_8(OH)_3 \cdot 2.9H_2O + 5OH^-$	$\log K_5 = -12$
TobH formation	$0.6667Ca^{2+} + H_2SiO_4^{2-} + 0.8333H_2O \rightarrow (CaO)_{0.6667}SiO2 \cdot 1.5H_2O + 0.6667OH^-$	$log K_6 = -5.33$

Table 3
Summary of the simulation parameter settings.

Simulation system ID	Reactive silica content in aggregate, %	Initial KK_{eq}^+, mol $\cdot$ L^{-1}	E_a, J $\cdot$ mol^{-1}	D_{agg}, m^2 $\cdot$ s^{-1}
$[S_{11}, S_{12}, S_{13}, S_{14}, S_{15}]$[a]	[6.58 10.41 20.15 32.41 40.91]	0.20	78,000	$4 \times 10^{-7} \times D_w$
$[A_{11}, A_{12}, A_{13}, A_{14}, A_{15}]$	[6.58 10.41 20.15 32.41 40.91]	0.38	78,000	$4 \times 10^{-7} \times D_w$
$[A_{21}, A_{22}, A_{23}, A_{24}, A_{25}]$	[6.58 10.41 20.15 32.41 40.91]	0.50	78,000	$4 \times 10^{-7} \times D_w$
$[A_{31}, A_{32}, A_{33}, A_{34}, A_{35}]$	[6.58 10.41 20.15 32.41 40.91]	0.75	78,000	$4 \times 10^{-7} \times D_w$
$[R_{11}, R_{12}, R_{13}, R_{14}, R_{15}]$	[6.58 10.41 20.15 32.41 40.91]	0.20	60,000	$4 \times 10^{-7} \times D_w$
$[R_{21}, R_{22}, R_{23}, R_{24}, R_{25}]$	[6.58 10.41 20.15 32.41 40.91]	0.38	60,000	$4 \times 10^{-7} \times D_w$
$[R_{31}, R_{32}, R_{33}, R_{34}, R_{35}]$	[6.58 10.41 20.15 32.41 40.91]	0.50	60,000	$4 \times 10^{-7} \times D_w$
$[R_{41}, R_{42}, R_{43}, R_{44}, R_{45}]$	[6.58 10.41 20.15 32.41 40.91]	0.75	60,000	$4 \times 10^{-7} \times D_w$
$[D_{11}, D_{12}, D_{13}, D_{14}, D_{15}]$	[6.58 10.41 20.15 32.41 40.91]	0.20	78,000	$1 \times 10^{-3} \times D_w$
$[D_{21}, D_{22}, D_{23}, D_{24}, D_{25}]$	[6.58 10.41 20.15 32.41 40.91]	0.20	78,000	$1 \times 10^{-4} \times D_w$
$[D_{31}, D_{32}, D_{33}, D_{34}, D_{35}]$	[6.58 10.41 20.15 32.41 40.91]	0.20	78,000	$1 \times 10^{-5} \times D_w$
$[D_{41}, D_{42}, D_{43}, D_{44}, D_{45}]$	[6.58 10.41 20.15 32.41 40.91]	0.20	78,000	$1 \times 10^{-6} \times D_w$
$[D_{51}, D_{52}, D_{53}, D_{54}, D_{55}]$	[6.58 10.41 20.15 32.41 40.91]	0.20	78,000	$1 \times 10^{-7} \times D_w$
$[D_{61}, D_{62}, D_{63}, D_{64}, D_{65}]$	[6.58 10.41 20.15 32.41 40.91]	0.20	78,000	$1 \times 10^{-8} \times D_w$

[a] In systems $[S_{11}, S_{12}, S_{13}, S_{14}, S_{15}]$, the difference is the reactive silica content in aggregate which is 6.58%, 10.41%, 20.51%, 32.41%, 40.91% respectively. The same principle applies to other simulation identities (IDs).

in the cement, is about 0.38 mol $\cdot$ L^{-1}. The concentration of K$_{eq}^+$ is the sum of the concentration of K$^+$ and the equivalent transferred K$^+$ concentration from Na$^+$. The average concentration was calculated by the total moles of the ion divided by the total volume of the nodes where the ion can diffuse into. The percentage of alkalis in portland cement is usually in the range of 0.2 to 1.3% Na$_2$Oe. Thus, percentages of 0.14%, 0.35%, 0.5%, 0.8% are chosen to study in our model, with an estimated K$_{eq}^+$ concentration of 0.2, 0.38, 0.50 and 0.75 mol $\cdot$ L^{-1} respectively calculated by the relationship between alkali concentration, w/c and Na$_2$O$_e$% proposed in [48] (assuming hydration degree is maximum). Instead of changing the clinker composition and redo the simulation to obtain the cement paste. we have artificially changed the concentration of K$_{eq}^+$ in the aforementioned simulated cement paste to the corresponding concentration while its spatial distribution was maintained. In fact, the distribution of the ions wouldn't change much since the the clinker composition is almost not changed by the Na$_2$Oe. The simulations systems for this part are referred to the system *A* series in the continuation of the paper.

The influence of silica microstructural disorder degree was realized by changing the dissolution activation energy of the silica (E_a). An activation energy of 78,000 J $\cdot$ mol^{-1} was used to represent the slowly-reactive silica while a value of 60,000 J $\cdot$ mol^{-1} was used to represent the highly-reactive silica. This has led to a dissolution rate change with a fold of 1000. The simulation systems for fast silica dissolution are referred to the system *R* series in the continuation of the paper. Except for these *R* series systems, the silica dissolution rate in all of other systems is the slowly one. In order to study the pessimum reactive silica content, different alkali concentrations are also considered when the silica is highly reactive.

The influence of aggregate porosity was realized by changing the ion diffusion coefficients in the aggregate. However, the aggregate porosity was not simulated from the 3D microstructure structure, but from an empirical equation based on the real mercury intrusion porosimetry (MIP) porosity to compensate the loss of the porosity during the simulation. According to Mihara et.al [49], the diffusion coefficients of ions in the aggregate D_{agg} can be estimated using the equation $D_{agg} = D_w \times \phi^{3.05}$, where D_w is the ions diffusion coefficient in water and ϕ is the MIP determined porosity. In this paper, six different diffusion coefficients from $1 \times 10^{-3} \times D_w$ to $1 \times 10^{-8} \times D_w$ were studied. The corresponding ϕ of the aggregate were 10.38%, 4.88%, 2.29%, 1.08%, 0.51%, 0.24% respectively. The simulations are referred to the system *D* series in the continuation of the paper.

Table 3 summarizes the simulation system identities (IDs) and the parameter settings in all of the mentioned systems. The second digit of the subscript represents a different reactive silica content in the aggregate. For example, $[S_{11}, S_{12}, S_{13}, S_{14}, S_{15}]$ correspond to the simulations with a reactive silica content in the aggregate of 6.58%, 10.41%, 20.51%, 32.41%, 40.91% respectively, an initial K$_{eq}$ concentration of 0.2 mol $\cdot$ L^{-1}, an activation energy of silica of 78,000 J $\cdot$ mol^{-1}, and diffusion coefficients of ions in the aggregate that are 4×10^{-7} times to the ones in water. The low alkali concentration was used in the systems because it is more easy for the system to reach its equilibrium constant. The silica was assumed to be the slowly-reactive one, which is more realistic. The ions diffusion coefficients in the aggregate D_{agg} equal to 4 $\times 10^{-7}$ times of that in the water calculated based on the real MIP porosity of the used limestone (0.8%). The same principle applies to the other systems. All of the simulations were done with a simulation time step $\Delta t = 3.6$ minutes. The initial average concentration of Ca^{2+} was 20 mmol $\cdot$ L^{-1} in all of the systems. Such a relative high Ca^{2+} concentration can help investigate the role of Ca^{2+} during ASR in a more comprehensive way including what happens during cement hydration since during hydration, the calcium concentration is very high. It should be noted that in field concrete, the Ca^{2+} concentration varies a lot depending on the mix design and ambient environment and is normally below 2.5 mmol $\cdot$ L^{-1} [11].

3. Simulation results

3.1. The chemical sequences of ASR

It is widely accepted that the dissolution of silica under the attack of OH$^-$ and cations such as K$^+$, Na$^+$ is the first step of ASR after it was firstly revealed by [50]. However, the subsequent reaction sequences are still under controversy and depends on many factors such as the calcium concentration in pore solution. In our former paper [28], by assuming a high calcium concentration in the pore solution (20 mmol $\cdot$ L^{-1}) we have investigated the influence of the silica dissolution rate on the ASR products formation sequence. It has been found that when the silica dissolves fast, KSH is formed immediately, while when the silica dissolves slowly, the formation of KSH is quite slow before the calcium is consumed to a low level. After that, KSH is massively formed. The confirmation of the simulation results is not discussed in the former paper due to a space limitation. In this paper, the comparison of the simulated sequence with the experimental data in literature will be given.

In this section, we will firstly present more details about the chemical sequence that is not discussed in our former paper such as the ions evolution. What's more, the influences of reactive silica content in aggregate, alkali concentration, silica microstructural disorder degree and aggregate porosity on the chemical sequences of ASR will be stated.

3.1.1. General discovery

Fig. 3(a) to Fig. 3(d) present the concentration evolution of the involved ions in system S_{15} with a reactive silica content of 40.91% in

aggregate within 540 days. Here, the concentration of each ion is the total moles of the ion divided by the total volume of the domain (1×10^{-9} L). The value is much lower than the real local concentration of the ions in the system since ions are not permeable in some of phases such as unhydrated cement. When the simulation starts, OH^- is diffused into the aggregate and causes the dissolution of silica as indicated by the decreasing of OH^- concentration in Fig. 3(a) and by the increasing of $H_2SiO_4^{2-}$ concentration in Fig. 3(b). Fig. 3(c) shows that the concentration of Ca^{2+} also decreases greatly after the simulation starts. This fast decrease is caused by the formation of TobH as indicated by the mass evolution (represented by M_V, unit $kg \cdot m^{-3}$) of TobH in Fig. 3(e). Here, M_V is defined as the total formed mass of the new phase (or total dissolved mass of the dissolving phase including silica, CH and C-S-H) divided by the total volume of the domain.

Obviously, there is a 'growth time' point for KSH to be formed in system S_{15} as indicated by the evolution of K_{eq}^+ in Fig. 3(d) and the mass evolution of KSH in Fig. 3(e). Before this 'growth time' point, no KSH is formed. After that, KSH begins growing in a stable fast rate while the growth of TobH is greatly decreased. By comparing the evolution of KSH

and the concentration change of Ca^{2+} in the system, it is found that this 'KSH growth time' point is consistent to the time when most of Ca^{2+} is depleted in the system (defined as the 'calcium depletion time' as shown in Fig. 3(c)). This finding is consistent to the findings in [43,51] that ASR gel is not formed until the calcium is consumed by the formation of C-S-H.

The reason behind is the different dependency of the thermodynamic state of KSH and TobH on Ca^{2+} and $H_2SiO_4^{2-}$. For KSH, its thermodynamic state depends more on the concentration of $H_2SiO_4^{2-}$, while the thermodynamic state of TobH depends more on the concentration of Ca^{2+}. In the beginning when the concentration of Ca^{2+} in the domain is high, once silica is dissolved, the solution can reach an over saturation state for TobH even the concentration of $H_2SiO_4^{2-}$ is still low. For KSH, it needs some time for $H_2SiO_4^{2-}$ to reach a high level to over saturate the solution as shown by the peak concentration at around 60 days in Fig. 3 (b).

Fig. 3(a) also shows that most of OH^- is consumed within 60 days in system S_{15}. After that, the concentration of OH^- keeps at a stable level. However, the low concentration of OH^- does not mean the dissolution of

(a)

(b)

(c)

(d)

(e)
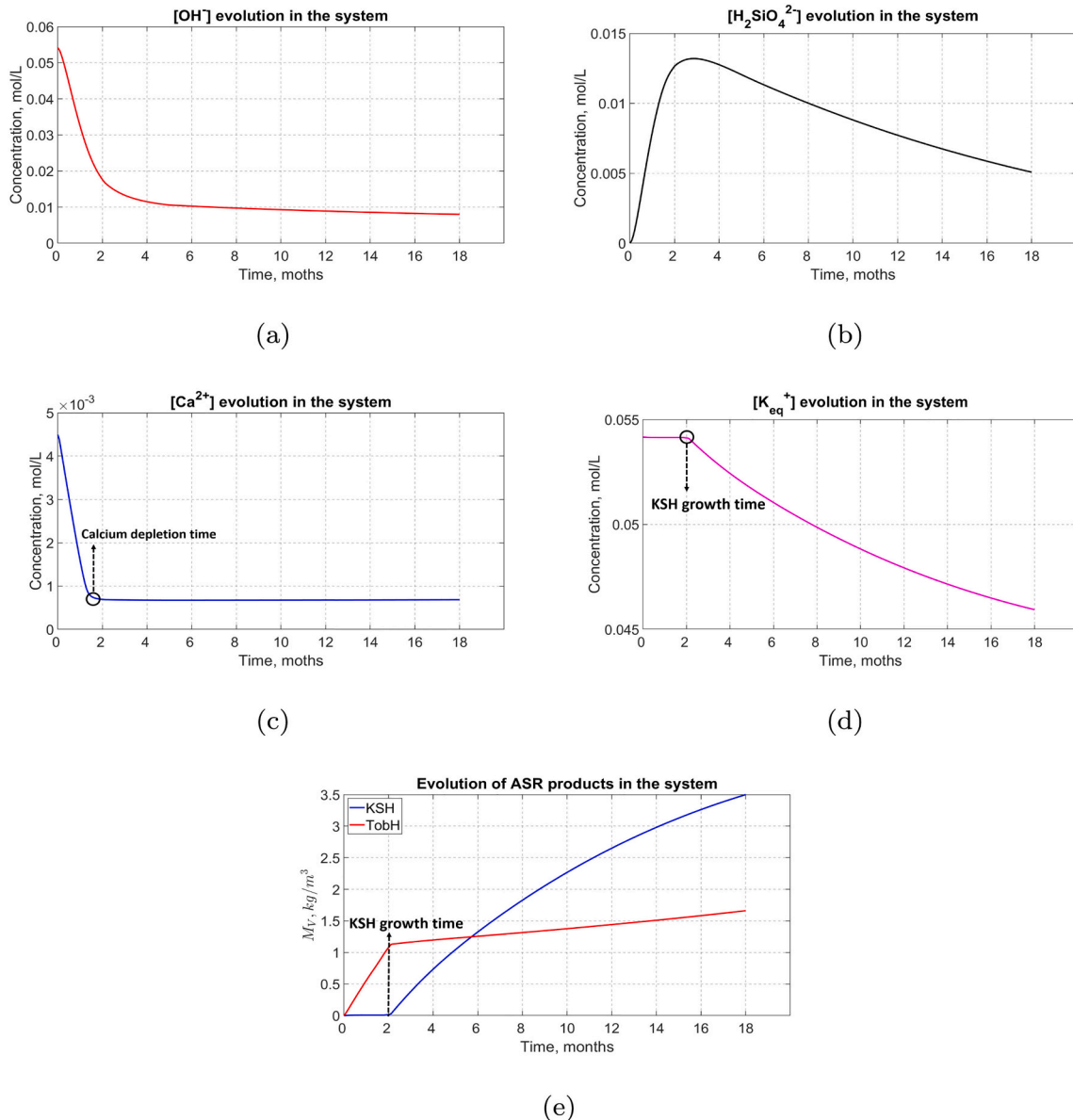
Fig. 3. The concentration evolution of OH^- (**a**), $H_2SiO_4^{2-}$ (**b**), Ca^{2+} (**c**) and K_{eq}^+ (**d**) in system S_{15} within 540 days; (**e**): Mass evolution of KSH and TobH represented by M_V in system S_{15} within 540 days.

silica is stopped. Due to the 'buffer effect' of CH and C-S-H dissolution in the cement paste, the silica keeps being dissolved at a lower rate. The influence of CH and C-S-H dissolution on ASR will be discussed in Section 3.2. This is also the reason why the concentration of Ca^{2+} is kept at a stable level in Fig. 3(c) while KSH is continuously formed at the same time. Nevertheless, the extra Ca^{2+} provided by the CH and C-S-H dissolution is not high enough for TobH to keep growing at a fast rate in this system as can be seen from the stable red curve after about 60 days in Fig. 3(e).

3.1.2. Effect of reactive silica content in aggregate

The simulation results from systems $[S_{11}, S_{12}, S_{13}, S_{14}, S_{15}]$ with different reactive silica contents in aggregate are used in this section. Fig. 4(b), the concentration evolution of Ca^{2+} in the above systems, shows that the calcium depletion time decreases as the reactive silica content increases in the aggregate. It is decreased by around 4 times in system S_{15} with 40.91% reactive silica in aggregate (around 50 days) compared with that in system S_{11} with 6.58% reactive silica in aggregate (around 200 days).

The difference is caused by the different amounts of dissolved silica. Fig. 4(c) shows that when the reactive silica content in the aggregate is high, OH^- is consumed faster than when the reactive silica content is low. Taking the time of 100 days as an example, the concentration of OH^- is dropped from 0.055 $mol \cdot L^{-3}$ to 0.012 $mol \cdot L^{-3}$ in system S_{15} (rose red curve in Fig. 4(c)), while its concentration is still as high as about 0.042 $mol \cdot L^{-3}$ in system S_{11} (blue curve in Fig. 4(c)). As a result, the concentration of $H_2SiO_4^{2-}$ reaches a very high level in a short time in system S_{15} as shown by the rose red curve in Fig. 4(d). Consequently, it is easier for KSH to grow in the system with a high reactive silica content in the aggregate. However, it can also be seen from all of the subfigures in Fig. 4 that the difference is not very big between system S_{14} and S_{15} (32.42% and 40.91% reactive silica in aggregate, green and rose red curve) in which the reactive silica content in the aggregate is higher than

30%. This means that the influence of the reactive silica content has an upper limit on the calcium depletion time or the KSH growth time. When the dissolved silica is very high, it is the other ions that limit the growth of KSH.

3.1.3. Effect of alkali concentration in cement paste

The simulation results from systems $[S_{15}, A_{15}, A_{25}, A_{35}]$ are used in this section, where the initial alkali concentrations in the cement paste are 0.2,0, 0.38, 0.50, 0.75 $J \cdot mol^{-1}$ respectively and 40.91% reactive silica content in the aggregate. The mass evolution of KSH, the concentration evolution of Ca^{2+} under different alkali concentrations, as shown in Fig. 5(a) and Fig. 5(b) respectively, indicate that the alkali concentration affects the growth rate of KSH a lot, but does not have a big effect on the calcium depletion time or the KSH growth time. The KSH growth time is the same in all of the systems which is around 50 days. Which means that the consumption time of Ca^{2+} to a low level that TobH stops growing and the accumulation time of $H_2SiO_4^{2-}$ to a high level for KSH growing are the same in all of the systems.

Similarly, the reason can again be found in the silica dissolution. As can be seen from the concentration evolution of $H_2SiO_4^{2-}$ in Fig. 5(d), the increase of the alkali concentration in the system increases the concentration of $H_2SiO_4^{2-}$. However, compared with Fig. 4(d), the increased rate (slope of the curves) is not as significant as that caused by the reactive silica content in aggregate. It is more obvious in Fig. 5(c) showing the evolution of OH^- that the decreasing rates of OH^- (slope of the curves) in all of the systems are almost the same. The time when the concentration of OH^- reaches a stable level also does not varies much between the systems, which is around 100 days. Therefore, the calcium depletion time or KSH growth time is not changed too much. Before 50 days, the concentration of Ca^{2+} is consumed to a low level in all of the systems. The same pattern that alkali concentration does not affect the KSH growth time or calcium depletion time has also been found in other systems with the same parameter setting except for different reactive
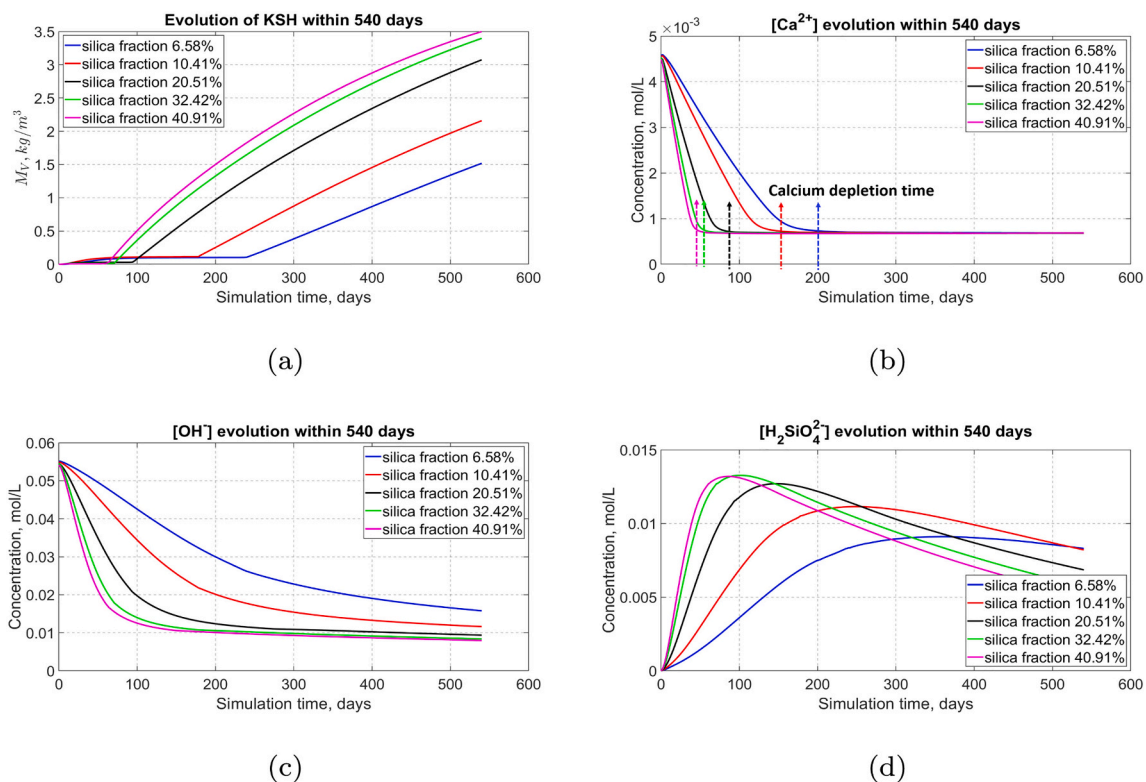
(a)

(b)

(c)

(d)

Fig. 4. Comparison of mass evolution of KSH and ions concentration evolution between systems with different reactive silica contents in aggregate within 540 days. (**a**): Mass evolution of KSH represented by M_V; (**b**): The concentration evolution of Ca^{2+}; (**c**): The concentration evolution of OH^-; (**d**): The concentration evolution of $H_2SiO_4^{2-}$.
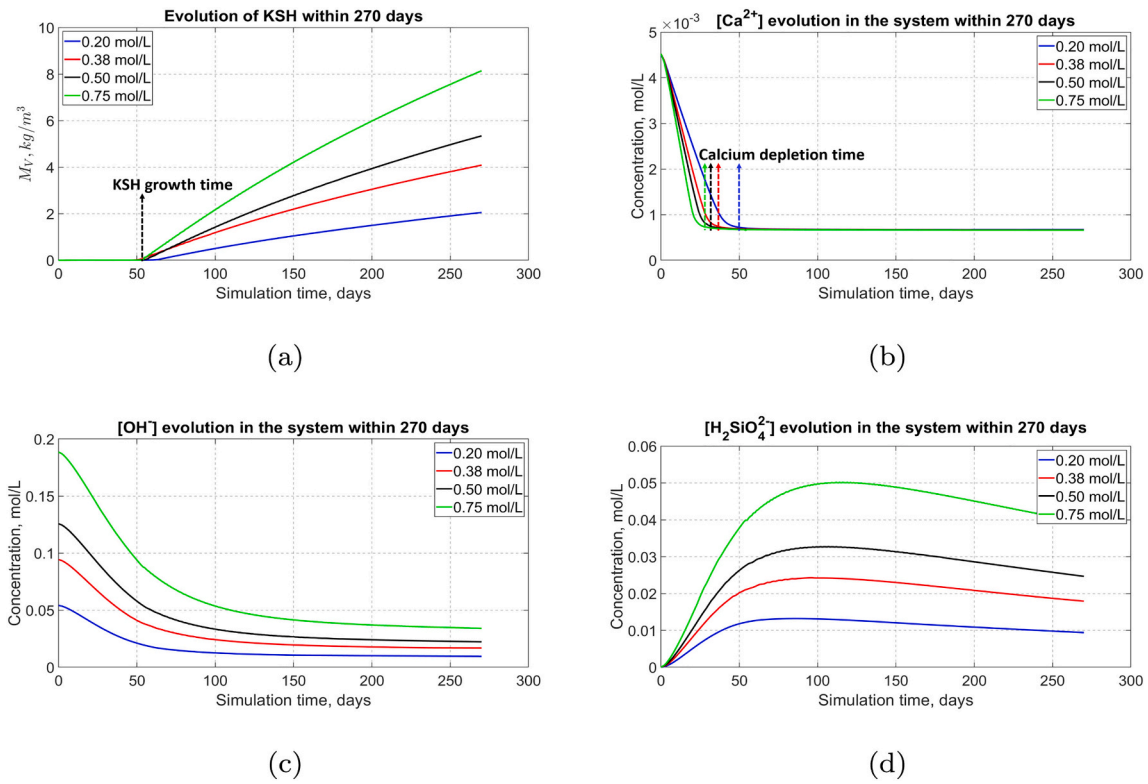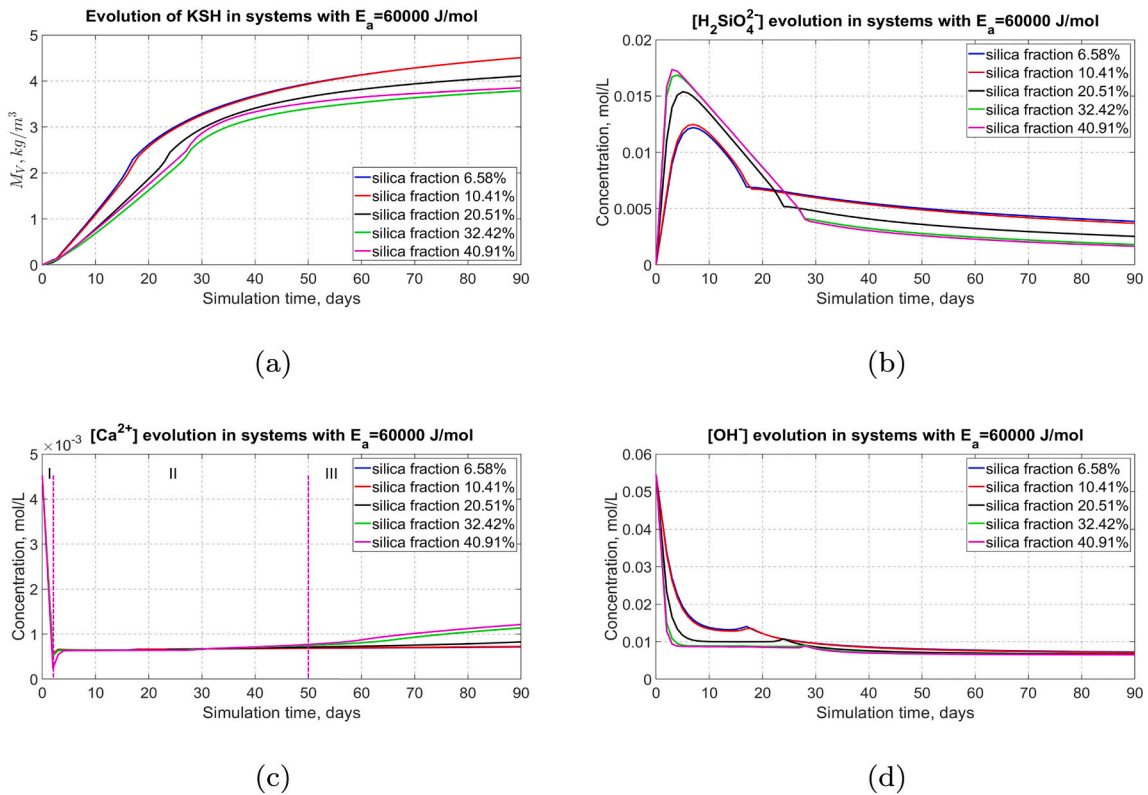
Fig. 5. Comparison of mass evolution of KSH and ions concentration evolution between systems with different alkali concentrations in cement paste within 270 days. (**a**): Mass evolution of KSH represented by M_V; (**b**): The concentration evolution of Ca^{2+}; (**c**): The concentration evolution of OH^-; (**d**): The concentration evolution of $H_2SiO_4^{2-}$.

Fig. 6. Mass evolution of ASR products and ions concentration evolution in systems with a silica dissolution activation energy of 60,000 $J \cdot mol^{-1}$ within 90 days. (**a**): Mass evolution of KSH represented by M_V; (**b**): The concentration evolution of $H_2SiO_4^{2-}$; (**c**): The concentration evolution of Ca^{2+}; (**d**): The concentration evolution of OH^-.

silica content in the aggregate (data are not presented due to space limitation).

3.1.4. Effect of silica microstructural disorder degree

As stated before, the influence of silica disorder degree was realized by changing the dissolution activation energy of the silica. The corresponding simulation systems are $[R_{11}, R_{12}, R_{13}, R_{14}, R_{15}]$ with a lower silica dissolution activation energy of 60,000 J · mol^{-1} and different reactive silica contents in aggregate respectively. The silica dissolution rate is increased by 1000 times compared with that in systems with a silica dissolution activation energy of 78,000 J · mol^{-1}. Data from all of the above five systems are used and compared with the corresponding systems with a high activation energy ($[S_{11}, S_{12}, S_{13}, S_{14}, S_{15}]$) in this section. Results show that the formation sequence of KSH and TobH is affected significantly by the silica dissolution rate.

Fig. 6(a) shows the mass evolution of KSH within 90 days. Obviously, when the dissolution rate is 1000 times faster, KSH is formed immediately in all of the systems no matter how much the reactive silica contents in aggregate is. There is no waiting time for KSH growth, which is caused again by the fast silica dissolution. The concentration of $H_2SiO_4^{2-}$ is soared up immediately after the simulation starts in all of the five systems as shown in Fig. 5 to supersaturate the solution for KSH formation. The growing rate of KSH gradually decreases to zero in all of the systems just after around 50 days which means the reaction has almost reached its equilibrium state, much faster than that when the silica dissolution rate is slow.

Fig. 6(c) shows the concentration evolution of the Ca^{2+} within 90 days in the above five systems. The change of Ca^{2+} can be divided into three stages in the systems where the reactive silica content is higher than 10.41% in the aggregate. Taking the system with 40.91% reactive silica in aggregate (rose red curve in Fig. 6(c)) as an example, in stage I, the Ca^{2+} decreases immediately after the simulation starts due to the consumption of both KSH and TobH so that there is no obvious calcium depletion time. In stage II, the concentration of Ca^{2+} increases a bit then keeps stable from around 8 days to 50 days. The increase is caused by the CH and C-S-H dissolution in the system. The stable period means the growing of KSH and TobH is fast, as indicated by the fast decrease of $H_2SiO_4^{2-}$ in Fig. 6(b) between around 8 days to 50 days. As a result, all the extra Ca^{2+} produced in this period are consumed. Subsequently in stage III, the concentration of Ca^{2+} starts increasing. It means the growth of KSH and TobH is decreased as indicated by the lower decreasing rate of $H_2SiO_4^{2-}$ in Fig. 6(b) after 50 days. However, the dissolution of CH and C-S-H is still triggered by the low ion concentration. Therefore, there is extra Ca^{2+} to be accumulated in the system until equilibrium state is reached. For systems R_{11} and R_{12} with 6.58% and 10.41% reactive silica in aggregate respectively (blue and red curve in Fig. 6(c)), it takes a longer time to increase its calcium concentration due to the relatively higher $H_2SiO_4^{2-}$ concentration in this stage as shown by the blue and red curve in Fig. 6(b).

The change of OH^- is different from that of Ca^{2+} as can be seen in Fig. 6(d). Most of OH^- is consumed within 8 days in all of the systems. After that, the concentration of OH^- is not increased again as Ca^{2+} but stays at a stable low level. This means that all the extra OH^- from CH and C-S-H is consumed by the silica dissolution.

3.1.5. Effect of aggregate porosity

The simulated results from systems $[D_{15}, D_{25}, D_{35}, D_{45}, D_{55}, D_{65}]$ are used for this section, where the aggregate porosity ϕ are 10.38%, 4.88%, 2.29%, 1.08%, 0.51%, 0.24% respectively and 40.91% silica in the aggregate. ϕ has a big influence on the calcium depletion time as shown in Fig. 7(b).

There is a calcium depletion time in all of the systems and it decreases as ϕ increases. But when ϕ is greater than 1.08%, the calcium depletion time does not change with ϕ anymore. When ϕ is less than or equal to 1.08%, Ca^{2+} is firstly consumed at a low rate and then remains

at a stable low level within 300 days as shown by the green, rose red and yellow curve. However, when ϕ is greater than 1.08%, the concentration of Ca^{2+} increases again after the stable period. The higher the porosity is, the earlier and faster the increase of concentration of Ca^{2+} is. Consequently, the concentration of Ca^{2+} in system D_{65} ($\phi = 10.38\%$) is the highest.

Correspondingly, the mass evolution of KSH shows a similar pattern to that of Ca^{2+}. There is a KSH growth time in the six systems as shown by the dash lines in Fig. 7(a), and it decreases as ϕ increases. Unlike stated before, this KSH growth time is not consistent to the calcium depletion time but longer than that when ϕ is less than or equal to 0.51%, indicating that the consumption of $H_2SiO_4^{2-}$ by TobH affects the accumulation of $H_2SiO_4^{2-}$ in these systems with low aggregate porosity.

The influence of ϕ is caused by the different diffusion rate of the ions in the aggregate. The higher ϕ is, the further and faster the ions can diffuse. Fig. 7(c) shows the distribution of average concentration of OH^- along X axis in the six systems just after 3 days. The average concentration is calculated as the total concentration of OH^- in the nodes where OH^- can diffuse into on each YOZ plane, divided by the total volume of those nodes. The dashed line in the figure distinguishes the aggregate zone (right part) and the cement paste zone (left part). As expected, the diffusion distance of OH^- in the aggregate increases as ϕ increases. When ϕ increases from 0.24% to 1.08%, the diffusion distance of OH^- increases from around only 10 μm (yellow curve) to 175 μm (green curve). When ϕ is greater than 1.08%, OH^- is able to diffuse into the whole aggregate zone and reaches a relatively high level just after 3 days. Consequently, more silica is dissolved and KSH is more early to be formed. Fig. 7(d) indicates that after 300 days, the concentration of $H_2SiO_4^{2-}$ in systems where ϕ is equal to or smaller than 1.08% is still high, while in systems where ϕ is higher than 1.08%, all the dissolved $H_2SiO_4^{2-}$ is consumed.

3.2. The role of CH and C-S-H dissolution

It can be seen from the previous simulation results that the dissolution of CH and C-S-H buffers the needed Ca^{2+} and OH^- in ASR. In this section, we will provide more details and investigate the influence of different factors on the dissolution of CH and C-S-H. One more simulation in system S_{15} without considering the CH and C-S-H dissolution is firstly done to derive some general patterns.

3.2.1. General discovery

Fig. 8(a) shows the reaction degree evolution in system S_{15} within 540 days with or without dissolution of CH and C-S-H in the cement paste. The reaction degree is the total mass of the dissolved silica divided by the total mass of silica in the aggregate. The red curve confirms our former discovery that without CH and C-S-H dissolution, the dissolution of silica stops after a short period which is around 80 days in system S_{15}. While with CH and C-S-H dissolution, the silica is dissolving continuously. Fig. 8(b) and (c) show the mass evolution of KSH and TobH in system S_{15} with or without CH and C-S-H dissolution respectively. Without the dissolution of CH and C-S-H in the cement paste, almost no KSH is formed and the TobH also stops growing after around 20 days. Fig. 8(d) shows that it is the dissolution of C-S-H rather than CH that buffers the ASR. C-S-H does not dissolve before the calcium depletion time.

The above results indicate that the C-S-H dissolution plays an important role in the process of ASR. Without C-S-H dissolution, only TobH is formed and the dissolution of silica will stop very soon. With C-S-H dissolution, both KSH and TobH can be formed and the dissolution of silica can continue all the time. In addition, no dissolution of CH in the cement paste is found in our simulation. This is corresponding to the experimental results obtained by Kim et.al [39] that the amount of CH in cement paste is not changed a lot during ASR. Another reason is that probably the dissolution rate of CH we adopted is too slow compared
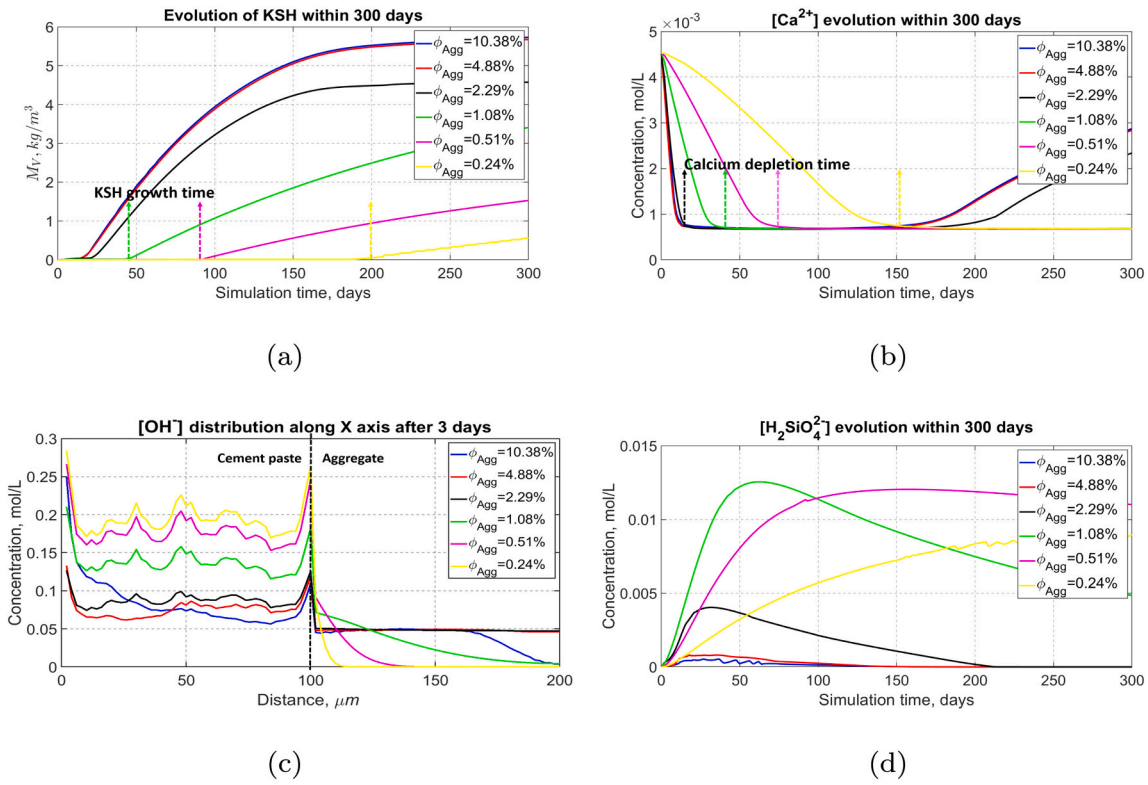
Fig. 7. (**a**): Mass evolution of KSH represented by M_V in systems with different aggregate porosity within 300 days; (**b**): The concentration evolution of Ca^{2+} 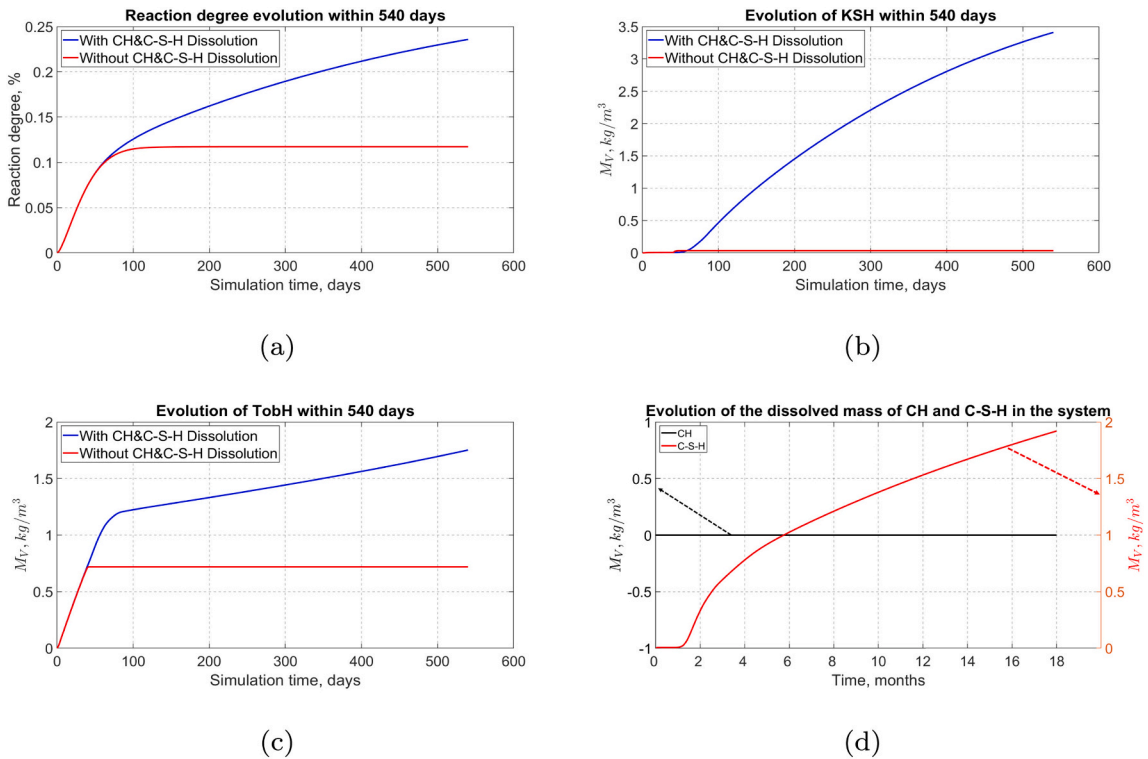in systems with different aggregate porosity within 300 days; (**c**): Distribution of average concentration of OH^- along X axis in systems with different aggregate porosity after 3 days; (**d**): The concentration evolution of $H_2SiO_4^{2-}$ in systems with different aggregate porosity within 300 days.

Fig. 8. (**a**): The reaction degree (the dissolved silica divided by the total mass of silica in the aggregate) evolution in system S_{15} with or without CH and C-S-H dissolution within 540 days; (**b**) and (**c**): Mass evolution of KSH (**b**), TobH (**c**) represented by M_V in system S_{15} with or without CH and C-S-H dissolution within 540 days; TobH (**d**): Mass evolution of dissolved CH and C-S-H represented by M_V in system S_{15} within 540 days.

with that of C-S-H. It is worth to mention that the dissolution of C-S-H will also produces extra $H_2SiO_4{}^{2-}$. However, we have found that compared with the dissolved $H_2SiO_4{}^{2-}$ from silica, the dissolved concentration of $H_2SiO_4{}^{2-}$ from C-S-H is two orders of magnitude smaller than that of the dissolution of silica, which is negligible and thus does not cause a big influence on ASR.

3.2.2. Effect of different factors on CH and C-S-H dissolution

The dissolution of CH in all of the systems is near to zero thus only the dissolution of C-S-H is presented in the section. Fig. 9(a) shows the mass evolution of the dissolved C-S-H in systems $[S_{11}, S_{12}, S_{13}, S_{14}, S_{15}]$ where the reactive silica content in the aggregate varies. It can be seen that the dissolved C-S-H increases as the reactive silica content increases. When the reactive silica content increases from 6.58% to 40.91%, the dissolved C-S-H increases by around 1.5 times from 1.2 to 1.8 kg $\cdot$ m^{-3}. This is a result to the change of the solution. As Ca^{2+}, OH^- in the pore solution is consumed by the reactive silica dissolution, KSH and TobH formation, the thermodynamic state for C-S-H becomes unstable, when the saturation degree for C-S-H formation is below 1, C-S-H will start dissolving. The more the ions are consumed, the larger the undersaturation degree is and thus the more C-S-H is dissolved. With the reactive silica content in aggregate increasing, more ions is consumed by the silica dissolution and formation of ASR products within the same time. Consequently, the mass of dissolved C-S-H increases.

Fig. 9(b) shows the mass evolution of the dissolved C-S-H in systems $[S_{15}, A_{15}, A_{25}, A_{35}]$ where the reactive silica content is 40.91% in the aggregate and the initial $K_{eq}{}^+$ concentration varies from 0.2 to 0.75 mol $\cdot$ L^3. Obviously, the dissolved C-S-H increases as the alkali concentration increases. With the alkali concentration increasing by 3.75 times from 0.2 to 0.75 mol $\cdot$ L^{-1}, the dissolved C-S-H increases from 1.2 to 4.8 kg $\cdot$ m^{-3}. The reason of the influence of the alkali concentration is the same to that of the reactive silica content in aggregate that more ions are

consumed in systems with high alkali concentration in the cement paste.

Fig. 9(c) shows the mass evolution of the dissolved C-S-H represented in systems $[R_{11}, R_{12}, R_{13}, R_{14}, R_{15}]$ with different reactive silica content in the aggregate and the silica dissolution is increased by 1000 times in all of the systems. It can be seen that differently from the pattern in Fig. 9 (a) where the silica dissolution rate is slow, the dissolved C-S-H shoots up in all of the systems after the simulations start. After 90 days, the dissolved C-S-H is much higher in all of the systems than that in the corresponding systems with a same reactive silica content but the silica dissolution rate is slower. Note to that the dissolved C-S-H is almost the same when the reactive silica content is below 10.5% and over 20.51% when the silica dissolution is 1000 times faster, which indicates the influence of silica microstructural disorder degree on C-S-H dissolution is much significant than the reactive content silica in aggregate. In addition, the release of C-S-H slows down after 30 days in all of systems. This is different from the situation when the silica dissolution rate is slow making the C-S-H dissolves in a relatively stable fast rate within 540 days as shown in Fig. 9(a). The same reason as stated before for the influence of high silica fraction on C-S-H dissolution can be referred again.

Fig. 9(d) shows the comparison of the mass evolution of the dissolved C-S-H in systems $[D_{15}, D_{25}, D_{35}, D_{45}, D_{55}, D_{65}]$ where the aggregate porosity varies from 0.24% to 10.38%. Obviously, the dissolved C-S-H increases as the aggregate porosity increases. The same pattern applies to the other D systems with different reactive silica content in the aggregate.

These simulation results indicate that the dissolution of C-S-H is a response to silica dissolution, the formation of KSH and TobH. The factors that increase the silica dissolution rate or the formation of ASR products will also increase the dissolution amount of C-S-H. Furthermore, the time when C-S-H starts dissolving is consistent with the calcium depletion time in all of the systems.

(a)

(b)

(c)

(d)
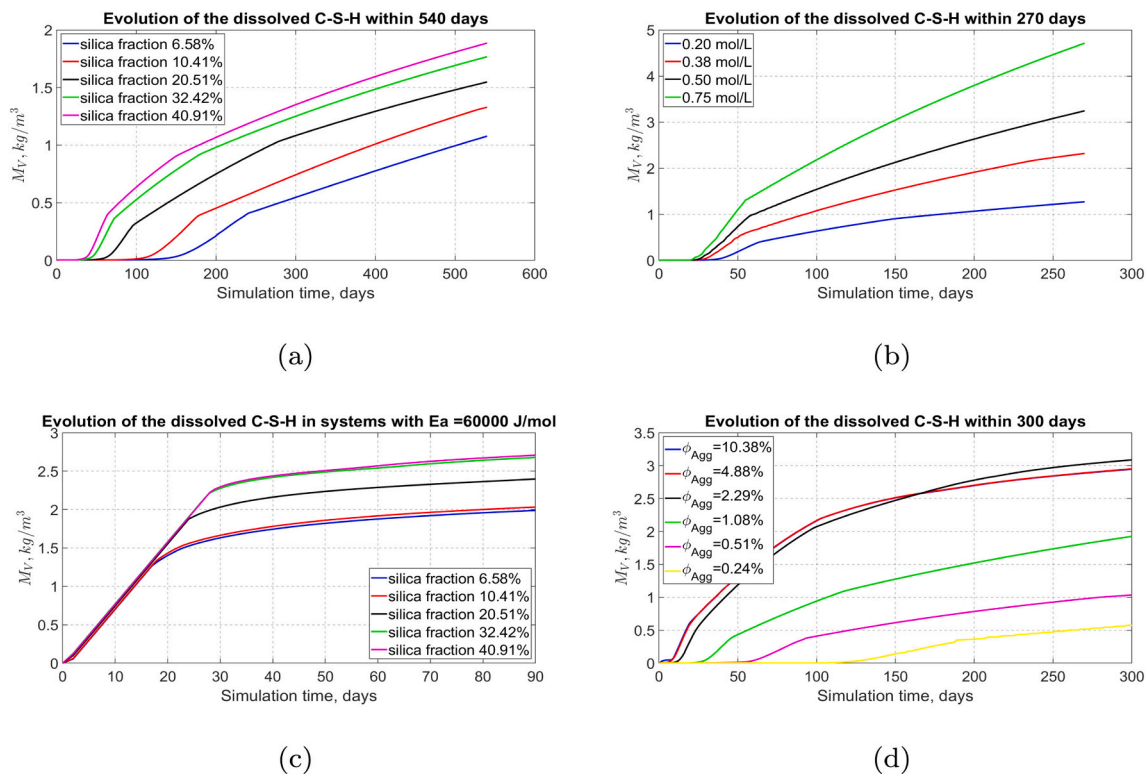
Fig. 9. (**a**): The mass evolution of the dissolved C-S-H represented by M_V in systems with different reactive silica content in aggregate within 540 days; (**b**): The mass evolution of the dissolved C-S-H represented by M_V in systems with different alkali concentration in cement paste within 270 days; (**c**): The mass evolution of the dissolved C-S-H represented by M_V in systems with a silica dissolution activation energy of 60,000 J $\cdot$ mol^{-1} within 90 days; (**d**): The mass evolution of the dissolved C-S-H represented by M_V in systems with different aggregate porosity within 300 days.

3.3. Location of KSH

Based on the fact that TobH does not contribute to the expansion, only the location of KSH is discussed in this section. In our former paper [28], we have simulated two typical distribution patterns of ASR products under different silica dissolution rate consistent to the experimental results. With fast dissolving silica, ASR products are located in the aggregate-cement paste zone in the beginning but very soon are formed all over in the cement paste. With slowly dissolving silica, the ASR products are formed inside the aggregate in a long-term. More details behind the phenomenon can be found in [28]. In this section, the influence of the other factors on the location of ASR products will be elaborated.

3.3.1. Effect of reactive silica content in aggregate

Simulation data from $[A_{31}, A_{33}, A_{35}]$ are used in this section, where the reactive silica contents in aggregate are 6.48%, 20.51% and 40.91% respectively, the initial alkali concentration is 0.75 mol $\cdot$ L^{-1} and aggregate porosity is 0.8%. The silica dissolution rate is the slowly one in these systems. Fig. 10 shows the mass distribution evolution of KSH on each YOZ plane along X axis (represented by $M_{V_{YOZ}}$, kg $\cdot$ m^{-3}) in the three systems within 270 days. The black dashed line in the figure distinguishes the cement paste zone and the aggregate zone. Here, $M_{V_{YOZ}}$ equals to the total mass of the KSH on each YOZ plane divided by the total volume of the domain. Fig. 10(a) shows that KSH is firstly formed inside the aggregate and then in the ITZ and cement paste after a long period when the reactive silica content in the aggregate is 6.58%. In system A_{33} with 20.51% reactive silica content in the aggregate (Fig. 10 (b)), before 120 days, only a small part of KSH is formed inside the aggregate near to the surface. After 120 days, KSH is distributed in the ITZ and cement paste zone. In system A_{35} with 40.91% reactive silica content in the aggregate (Fig. 10(c)), almost no KSH is formed inside the aggregate compared with that formed in the ITZ and cement paste from the beginning. Obviously, with the reactive silica content in the aggregate increasing, the location of KSH shifts from inside of the aggregate to the ITZ and cement paste zone. But given enough time, KSH can also be found in the ITZ and cement paste zone.

The different location is caused by the different concentration of the dissolved $H_2SiO_4^{2-}$. In system A_{31}, the dissolved $H_2SiO_4^{2-}$ is smaller than that in system A_{33} and A_{35} as the reactive silica content is small. The dissolved $H_2SiO_4^{2-}$ at the surface of aggregate is mostly consumed by the formation of TobH, while the dissolved $H_2SiO_4^{2-}$ inside the aggregate is accumulated and needs a long time to diffuse out into the ITZ and cement paste considering the aggregate porosity is very low (0.8%). Thus, KSH is firstly formed inside the aggregate and then in the ITZ and cement paste. However, when the reactive silica content increases to 20.51%, the dissolved $H_2SiO_4^{2-}$ concentration at the surface of the aggregate is high enough for TobH formation and for diffusion into the ITZ and cement paste. At the same time, the silica inside the aggregate is not dissolved too much because most of OH$^-$ is consumed at the aggregate surface and could not diffuse too far into the aggregate.

However, the location of KSH in system A_{31} can still be affected by the aggregate domain size since the ions are diffused back when they reach the east wall of the aggregate thus the ions concentration in domain is increased. Therefore, a simulation with the same parameter settings as system A_{31} except for an aggregate domain size of $100 \times 200 \times 100 \ \mu m^3$ is done. The simulation results (not presented due to space limitation) excludes the size effect on the location of KSH in system. The same pattern as in A_{31} is found that KSH is firstly formed inside the aggregate and then in the ITZ and cement paste zone.

3.3.2. Effect of alkali concentration in the cement paste

Simulation data from $[S_{11}, A_{11}, A_{21}]$ are used in this section, where the reactive silica contents in aggregate is 6.58%, the initial alkali concentration in the cement paste are 0.20, 0.38, 0.50 mol $\cdot$ L^{-1} respectively and the aggregate porosity is 0.8%.

The mass distribution evolution of KSH on YOZ plane along X axis in the three systems is shown in Fig. 11. Compared with the reference Fig. 10(a) where the alkali concentration is 0.75 mol $\cdot$ L^{-1}, it is obvious that the alkali concentration does not influence the location of KSH

(a)

(b)

(c)
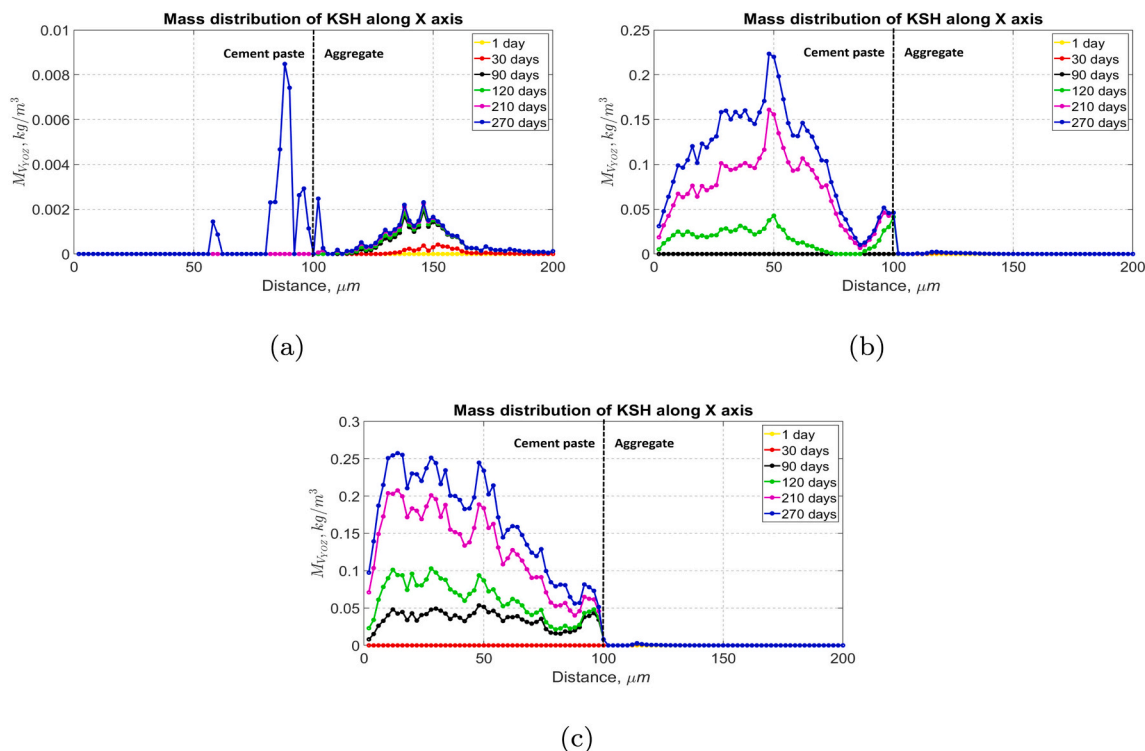
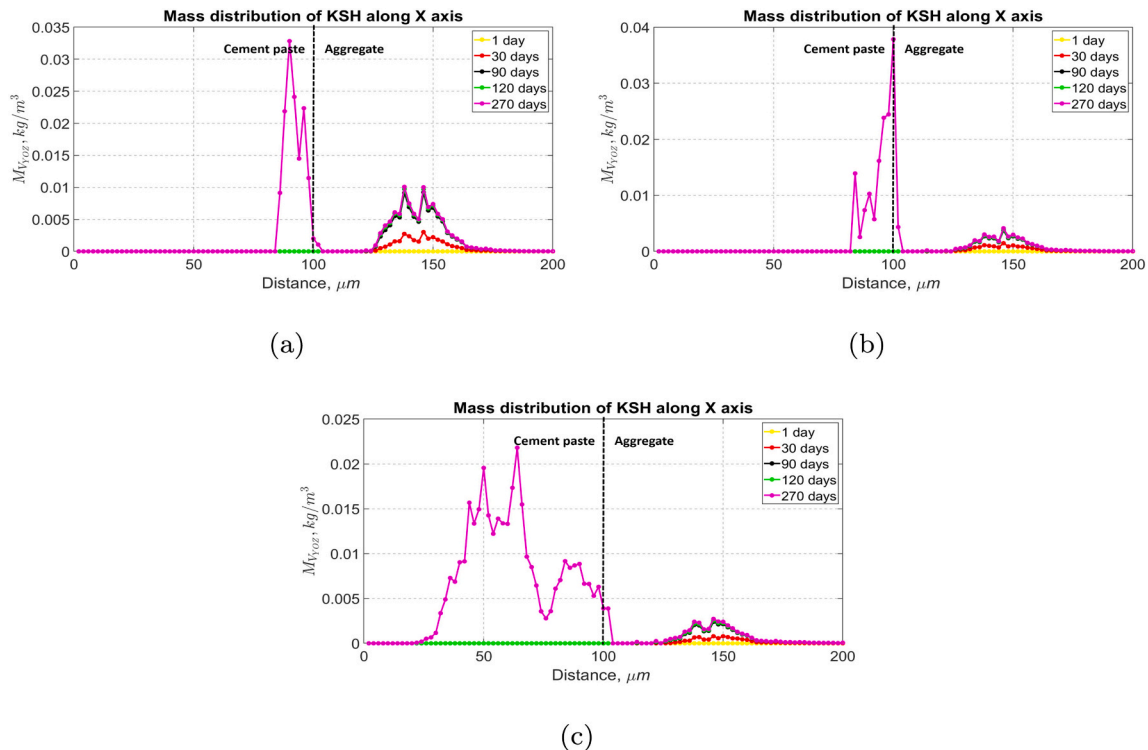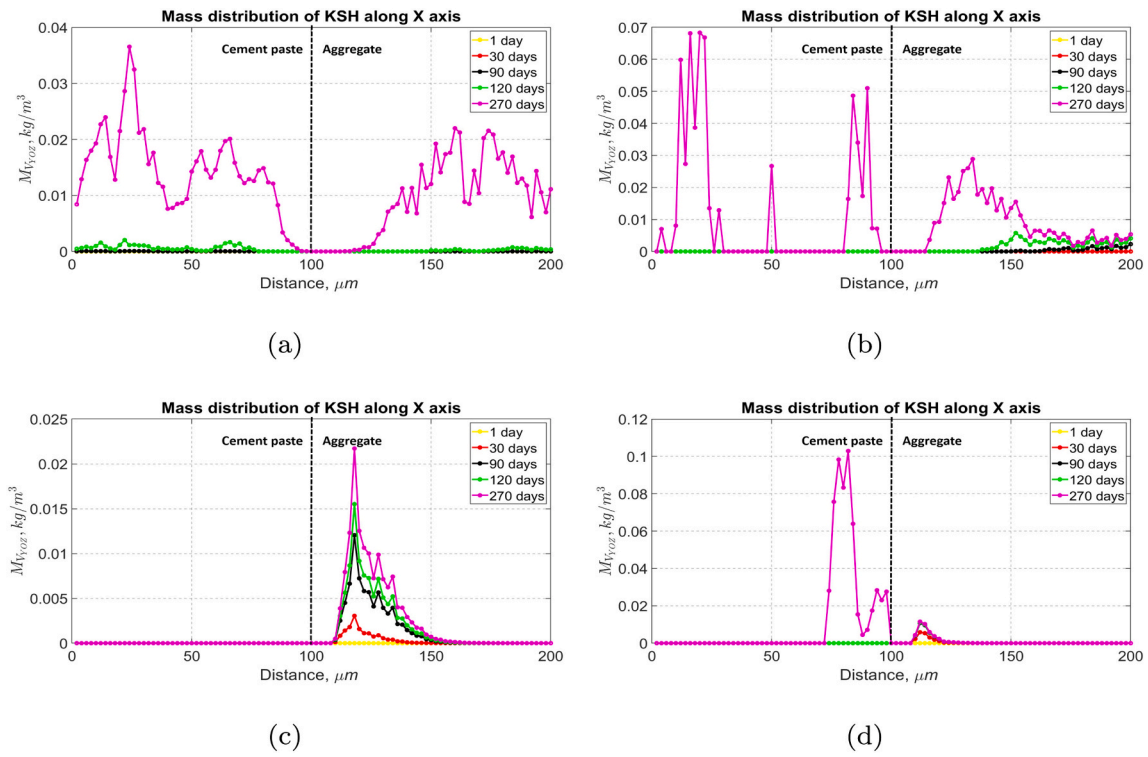**Fig. 10.** The mass distribution evolution of KSH along X axis represented by $M_{V_{YOZ}}$ in systems with different reactive silica contents in aggregate. (**a**): in system A_{31} with 6.58% reactive silica content; (**b**): in system A_{33} with 20.51% reactive silica content; (**c**): in system A_{35} with 40.91% reactive silica content.

much when the reactive silica content in aggregate is low that KSH is formed firstly inside the aggregate and gradually its main location shifts into the ITZ and cement paste. One small difference is that the KSH is more accumulated inside the ITZ when the alkali concentration is smaller or equal to $0.5 \text{ mol} \cdot \text{L}^{-1}$. The location is not influenced either in systems where the reactive silica content in aggregate is high. Apparently, the contribution of alkali concentration to the location of KSH is not as large as the effect of the reactive silica content.

3.3.3. Effect of aggregate porosity

Simulation data from systems $[D_{11}, D_{31}, D_{51}]$ are used in this section, where the reactive silica content in aggregate is 6.58% and aggregate porosity ϕ is 10.38%, 2.29% and 0.51% respectively. The initial alkali concentration in cement paste is $0.75 \text{ mol} \cdot \text{L}^{-1}$. Fig. 12 shows the mass distribution evolution of KSH along X axis. It can be seen that ϕ has a big influence on the location of KSH. With the reactive silica content in aggregate being only 6.58%, when ϕ is higher than or equal to 2.29%, KSH is formed inside aggregate, ITZ and cement paste very soon due to the fast diffusion of the ions in the system. While when ϕ is below or equal to 0.51%, KSH is only formed inside the aggregate near to its surface even after 270 days. Simulation results also show that when the reactive silica content is high (higher than 10.41%), the influence of ϕ on the location of KSH is different. With a high reactive silica content, the main location of KSH tends to shift to the inside the cement paste when ϕ is 0.51% as shown in Fig. 12(d). When ϕ is higher than or equal to 2.29% (not presented due to space limitation), KSH is inside aggregate, ITZ and cement paste and aggregate from the beginning. The above analysis indicates that when the aggregate porosity is higher than or equal to 2.29%, the location of KSH is always inside aggregate, ITZ and cement paste no matter how much the reactive silica content in aggregate is. When the aggregate porosity is smaller than 2.29%, the location of KSH depends on the reactive silica content.

3.4. Pessimum highly-reactive silica content

Certain aggregates containing highly-reactive forms of silica have been reported to exhibit a pessimum aggregate content [4,12,50] at mesoscale or macroscale. Our simulation results investigated this phenomenon at microscale when the silica is assumed to be highly reactive.

Simulation data from systems $[R_{41}, R_{42}, R_{43}, R_{44}, R_{45}]$ where the alkali concentration is $0.75 \text{ mol} \cdot \text{L}^{-1}$ and the reactive silica contents are 6.58%, 10.41%, 20.51%, 32.42% and 40.91% respectively. The silica is the highly-reactive one. Fig. 13(a) shows the relationship between the reactive silica content in aggregate and the free expansion obtained from the five systems. The free expansion is the total extra volume divided by the total volume of the domain. It can be seen that the free expansion decreases with increasing reactive silica content. The same phenomenon happens in other systems $[R_{31}, R_{32}, R_{33}, R_{34}, R_{35}]$ and $[R_{21}, R_{22}, R_{23}, R_{24}, R_{25}]$ where only the alkali concentration is different.

The reason behind is that different amounts of KSH and TobH are formed when the silica dissolution rate is fast. As can be seen from Fig. 13(b) and (c), when the reactive silica content in the aggregate is high, more TobH and less KSH are formed in the system while when the reactive silica content is low, more KSH is formed. Bearing in mind that the expansion ratio of TobH is much less than that of KSH, no wonder the expansion is greatly reduced.

4. Discussion

4.1. Fundamentals of ASR

4.1.1. Role of calcium

According to the above simulation results, it is confirmed that the presence of calcium has a significant influence on ASR. And the observed role of calcium is more accurate than the ones described in literature, showing that calcium either suppresses [22] or facilitates ASR [25]. Without extra calcium provided by the dissolution of C-S-H or CH in the

(a)

(b)

(c)

Fig. 11. The mass distribution evolution of KSH along X axis represented by $M_{V_{YOZ}}$ in systems with different alkali concentrations in the cement paste within 270 days. (**a**): in system S_{11} with $0.20 \text{ mol} \cdot \text{L}^{-1}$ alkali concentration; (**b**): in system A_{11} with $0.38 \text{ mol} \cdot \text{L}^{-1}$ alkali concentration; (**c**): in system A_{21} with $0.50 \text{ mol} \cdot \text{L}^{-1}$ alkali concentration.

(a)

(b)

(c)

(d)

Fig. 12. The mass distribution evolution of KSH along X axis represented by $M_{V_{YOZ}}$ in system D_{11} with $\phi = 10.38\%$ (**a**), system D_{31} with $\phi = 2.29\%$ (**b**), system D_{51} with $\phi = 0.51\%$ (**c**) and system D_{53} with $\phi = 0.51\%$ and 20.51% reactive silica content (**d**) within 270 days.
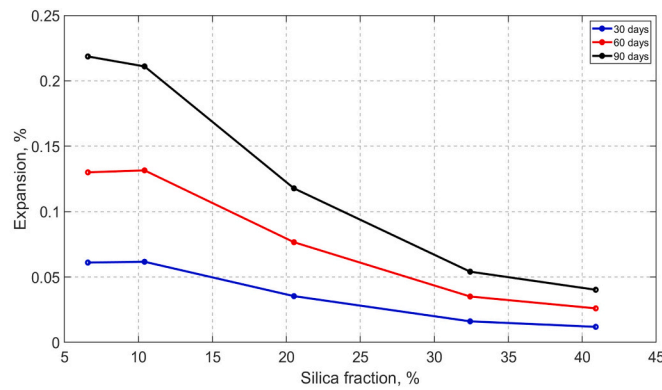
(a)
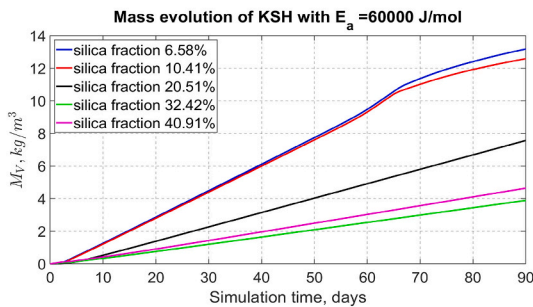
(b)
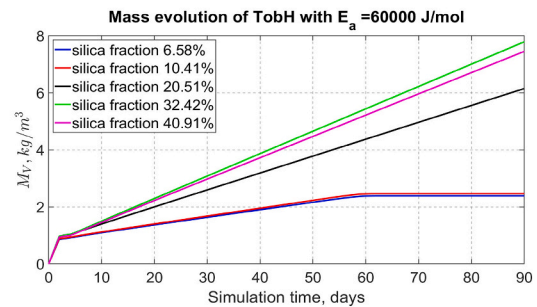
(c)

Fig. 13. (**a**): The relationship between reactive silica content in aggregate and expansion in systems with high silica dissolution rate within 90 days; (**b**): The mass evolution of KSH represented by M_V in system $[R_{41}, R_{42}, R_{43}, R_{44}, R_{45}]$ within 90 days; (**c**): The average density evolution of TobH in system $[R_{41}, R_{42}, R_{43}, R_{44}, R_{45}]$ within 90 days.

cement paste, ASR will stop soon after the initial calcium in the system is consumed. What's more important is that the calcium concentration should be kept at a low level for ASR to continue. As long as the concentration of Ca^{2+} is higher than a level (an equivalent concentration of around 4 mmol $\cdot$ L^{-1} in the pore solution based on the simulation results), the formation of KSH is inhibited and it is more easy for TobH to be formed due to its thermodynamic dependency on the calcium ions, which is also called the 'pozzolanic effect' [39,52,53]. Except for a low Ca^{2+}, the concentration of the dissolved silica should exceed a threshold level (an equivalent concentration of around 60 mmol $\cdot$ L^{-1} in the pore solution based on the simulation results) for KSH to be formed. Furthermore, the alkali concentration should also be higher than a threshold level, an equivalent concentration of around 0.16 mol $\cdot$ L^{-1} in the pore solution based on the equilibrium state in the simulations. Therefore, except for high moisture, three conditions are found for KSH to be formed in this paper: (a) a high concentration of $H_2SiO_4^{2-}$, (b) a low Ca^{2+} concentration and (c) a high level of alkali concentration. A similar conclusion is originally proposed by Hou et al. [43] and extended by Kim [51], based on the results in a simplified system where CH solid powder and silica powder were immersed in a high alkali solution. They found that ASR gel is not formed until all of the CH is consumed by the formation of C-S-H. In their studies, the ASR gel, are assumed to be calcium free so the conclusion was made that ASR gel could be generated continuously even there is no extra calcium. However, calcium is present in the ASR product in reality, which is considered in our model based on the most recent results of Shi et al. [3,42]. Therefore, the buffer effect of CH and C-S-H dissolution is a necessary condition for ASR.

4.1.2. Chemical sequence of ASR

Based on the simulation results, a general comprehensive chemical sequence of ASR in the early stage before cracking can be derived:

(1) Firstly the reactive silica dissolves under the attack of OH$^-$ that comes from the cement paste;

(2) The Ca^{2+} concentration in the pore solution of concrete varies a lot at a level of mmol $\cdot$ L^{-1} [11,54] depending on the mix design and ambient environment. When the concentration is below around 4 mmol $\cdot$ L^{-1}, no TobH or a small amounts of TobH will be formed. When the concentration is above the level, TobH are formed immediately after the silica dissolves. At the same time, $H_2SiO_4^{2-}$ is accumulated in the system while the concentration of Ca^{2+} keeps dropping by the consumption of TobH. This stage is characterized by the calcium depletion time;

(3) When the concentration of Ca^{2+} is low and $H_2SiO_4^{2-}$ is higher than 60 mmol $\cdot$ L^{-1} and alkali concentration is higher than 0.16 mol $\cdot$ L^{-1}, KSH starts being formed and the growth rate of TobH plunges. This stage is characterized by a KSH growth time;

(4) The dissolution of CH or C-S-H in cement paste buffers Ca^{2+} and OH$^-$ in the pore solution so that KSH can keep growing at a high rate and silica can keep dissolving.

(5) ASR stops until the amount of alkali in the pore solution is not high enough to oversaturate the pore solution for KSH formation. However, if the alkalies in the ASR products can be replaced by calcium as proposed in literature [50,55,56], ASR does not appear to reach a maximum value.

Compared with the proposed chemical sequence in literature [25,39,43,50] as mentioned in Section 3.1.1, the role of extra Ca^{2+} and OH$^-$ in ASR is clarified in the above chemical sequence. Due to the buffer effect, OH$^-$ is always reachable and it is other factors that stop ASR such as the low concentration of alkali. This raises an interesting assumption that maybe the rate-limit step of ASR is the dissolution of CH or C-S-H in the cement paste instead of the silica dissolution which is widely agreed in the present literature [39,57].

Many factors can affect the chemical sequence. Adopting a relative

high calcium concentration in the model, our simulation results show that the calcium depletion time and KSH growth time are influenced by some of the investigated factors such as the reactive silica fraction, the silica microstructural disorder degree, the aggregate porosity, while not affected much by the others such as the alkali concentration once it beyond the threshold concentration. The nature behind the influence of these factors is the change of the silica dissolution rate. Since a threshold concentration of dissolved silica and a low calcium concentration are necessary for the formation of KSH, any factor that can increase the silica dissolution rate would accelerate the consumption of the initial high concentration of calcium and the accumulation of the dissolved silica concentration. As a result, the calcium depletion time and the starting time of KSH growth are shortened, making ASR to happen earlier and faster. As stated in our former paper [28] and in [51,58], the silica dissolution rate is proportional to the dissolution constant, the silica surface area, the pH (a power of 0.5), the ionic strength (a power of 0.2) and the undersaturation degree. An increase of the reactive silica fraction in the aggregate or the silica microstructural disorder degree or the aggregate porosity would result in an increase of the silica surface area, the rate constant, and the pH inside the aggregate plus the silica surface area (because the diffusion distance of OH$^-$ is increased) respectively. Consequently, the calcium depletion time and the starting time of KSH growth decrease or even disappear when the dissolution rate is high enough. On the other hand, the increase of alkali concentration is unable to make a big change of the dissolution rate so that these two characteristic times (calcium depletion time and KSH growth time) are not influenced a lot.

4.1.3. Initial location of ASR products

whether the initial products or the initial expansive sites are in the aggregate-cement paste interface zone (so-called reaction rim around the reactive aggregate) or inside the aggregate (in the pre-exist cracks or defects, formation of gel pockets, formation of gel vein etc.) has been in dispute in literature. The formation of reaction rim around highly-reactive aggregate leading to cracking from the ITZ and cement paste has been observed in [59,60], while cracking from the inside of the aggregate has also been reported in [61,62], In 2021, Miura, M. et al. [63] argued that these two different expansion patterns depends on the homogeneity of the aggregate. Sometimes these two patterns can occur in a same aggregate. This paper is able to give some insights about the origin of the expansion considering as many influential factors as much.

Combining the simulation results in this paper and the simulation results in our former paper [28] where the influence of silica microstructural disorder degree on the location of ASR products is clarified, three characteristic location patterns of ASR products can be concluded: (1) inside aggregate; (2) inside ITZ and cement paste; (3) inside aggregate, ITZ and cement paste. The determining factors behind are the silica dissolution rate and the aggregate porosity.

When the aggregate porosity is very low (porosity less than or equal to 1.08% in this paper) and the silica dissolution rate is very fast, OH$^-$ is consumed quickly by the silica dissolution in the aggregate-cement paste zone enabling the dissolved silica to diffuse into the cement paste very easily. Meanwhile, the low concentration of OH$^-$ makes it is unable to diffuse into the aggregate further. As a result, ASR products are mainly formed in the ITZ or in the cement paste. This is what happens when the silica microstructural disorder degree is high or the silica fraction is very high (higher than or equal to 20.51% based on the simulation results). When the silica dissolves slowly, OH$^-$ is consumed in a slow rate so that its high concentration makes it possible to diffuse into the aggregate. As a result, the reaction front is distributed all over inside of the aggregate. This is what happens when the silica microstructural disorder degree is small or the silica fraction is low (lower or equal to 10.41% based on the simulation results).

When the aggregate porosity is high (porosity higher than or equal to 2.29% in this paper), OH$^-$ can diffuse into the aggregate much easier and the dissolved silica is also able to diffuse out from the aggregate

reactive silica dissolves slowly, there is an apparent calcium depletion time or a KSH growth time when the initial calcium concentration is higher than around 4 mmol · L^{-1} in the pore solution. TobH is formed firstly until the calcium depletion time. Then KSH will start growing. With the silica dissolution rate increasing, the calcium depletion time or the KSH growth time decrease and even disappear if the silica dissolution rate is fast enough. ASR stops when the amount of alkalis in the pore solution is not high enough.

- The location of ASR products is controlled by the silica dissolution rate and the aggregate porosity. When the silica dissolution rate and the aggregate porosity are both small, ASR products are formed inside the aggregate. With increasing silica dissolution rate, the location of ASR products shifts from the inside of aggregate to the ITZ and cement paste. With the porosity increasing, the location shifts from inside aggregate (low silica dissolution rate) or inside ITZ and cement paste (high silica dissolution rate) to inside ITZ, cement paste and aggregate from the beginning due to the easier access of the ions into the aggregate.

- High alkali concentration and high temperature are used in the laboratory experiments in order to accelerate ASR. According to our work, the high alkali concentration would not affect the chemical fundamental of ASR. But a higher temperature probably will change the formation location of ASR products as the silica dissolution rate is much higher and as a result, the cracking mechanism may be different from that in field concrete.

- When the silica is highly reactive, a pessimum silica content was found in literature [8,9] beyond which the ASR-induced expansion does not increase but decrease with the reactive silica content increasing. The reason revealed by this paper is that more TobH is formed when the reactive silica content is high. Combined with the proposed mechanisms in literature [4,64], a comprehensive mechanism to explain the pessimum effect in a long term in field concrete is derived. In real concrete with a highly reactive aggregate used, part of the alkalis are reacted by the dissolved silica during the hardening period. After the hardening of concrete, 'pozzolanic effect' happens. Most of the dissolved silica is reacted by the formation of C-S-H. At the same time, the dissolution of the CH and C-S-H in the cement paste near to the aggregate-cement paste surface is triggered to buffer the Ca^{2+}. But most of the dissolved calcium are used up for the formation of C-S-H and ASR products in the aggregate-cement zone. As a result, less calcium is able to diffuse into the aggregate so that the reaction rim (C-S-H) inside the aggregate is reduced. According to Ichikawa [64] and Maraghechi et al. [68], this reaction rim around the reactive silica mineral acts as a barrier for ASR gel accumulation, favouring expansive pressure and potentially leading to crack formation.

CRediT authorship contribution statement

Xiujiao Qiu: Conceptualization, Methodology, Software, Validation, Formal analysis, Investigation, Data curation, Writing – original draft, Visualization. **Jiayi Chen:** Software, Methodology. **Guang Ye:** Resources, Supervision, Writing – review & editing. **Geert De Schutter:** Resources, Supervision, Project administration, Writing – review & editing, Funding acquisition.

Declaration of competing interest

The authors declare that they have no known competing financial interests or personal relationships that could have appeared to influence the work reported in this paper.

References

[1] F. Rajabipour, E. Giannini, C. Dunant, J.H. Ideker, M.D. Thomas, Alkali–silica reaction: current understanding of the reaction mechanisms and the knowledge gaps, Cem. Concr. Res. 76 (2015) 130–146.

[2] B. Fournier, M.-A. Bérubé, Alkali-aggregate reaction in concrete: a review of basic concepts and engineering implications, Can. J. Civ. Eng. 27 (2000) 167–191.

[3] Z.G. Shi, B. Lothenbach, The role of calcium on the formation of alkali-silica reaction products, Cem. Concr. Res. 126 (2019), 105898.

[4] D.W. Hobbs, Alkali-silica Reaction in Concrete, Thomas Telford Publishing, 1988.

[5] S. Poyet, A. Sellier, B. Capra, G. Foray, J.-M. Torrenti, H. Cognon, E. Bourdarot, Chemical modelling of alkali silica reaction: influence of the reactive aggregate size distribution, Mater. Struct. 40 (2007) 229.

[6] C.F. Dunant, K.L. Scrivener, Effects of aggregate size on alkali–silica-reaction induced expansion, Cem. Concr. Res. 42 (2012) 745–751.

[7] A. Binal, The pessimum ratio and aggregate size effects on alkali silica reaction, Prog. Earth Planet. Sci. 15 (2015) 725–731.

[8] A. Shayan, The 'pessimum' effect in an accelerated mortar bar test using 1M NaOH solution at 80C, Cem. Concr. Compos. 14 (1992) 249–255.

[9] F. Bektas, L. Turanli, T. Topal, M. Goncuoglu, Alkali reactivity of mortars containing chert and incorporating moderate-calcium fly ash, Cem. Concr. Res. 34 (2004) 2209–2214.

[10] M.A.T.M. Broekmans, The Alkali-silica Reaction: Mineralogical and Geochemical Aspects of Some Dutch Concretes and Norwegian Mylonites, 2002. Ph.D. thesis.

[11] M.D. Thomas, B. Fournier, K.J. Folliard, et al., Alkali-aggregate Reactivity (AAR) Facts Book., Technical Report, United States, Federal Highway Administration. Office of Pavement Technology, 2013.

[12] T.E. Stanton, Expansion of concrete through reaction between cement and aggregate, Trans. Am. Soc. Civ. Eng. 107 (1942) 54–84.

[13] S. Diamond, Effects of microsilica (silica fume) on pore-solution chemistry of cement pastes, J. Am. Ceram. Soc. 66 (1983), C–82.

[14] T. Kim, Alkali-silica reaction: chemical mechanism, thermodynamic modeling, and effects of lithium ions, Ph.D. thesis, Purdue University, 2013.

[15] S. Multon, A. Sellier, M. Cyr, Chemo–mechanical modeling for prediction of alkali silica reaction (ASR) expansion, Cem. Concr. Res. 39 (2009) 490–500.

[16] X.X. Gao, S. Multon, M. Cyr, A. Sellier, Alkali–silica reaction (ASR) expansion: pessimum effect versus scale effect, Cem. Concr. Res. 44 (2013) 25–33.

[17] D. Stark, in: The moisture condition of field concrete exhibiting alkali-silica reactivity, specialPublication 126, 1991, pp. 973–988.

[18] L.-O. Nilsson, Moisture effects on the alkali-silica reaction, in: Proceedings of, 1983.

[19] S. Poyet, A. Sellier, B. Capra, G. Thèvenin-Foray, J.-M. Torrenti, H. Tournier-Cognon, E. Bourdarot, Influence of water on alkali-silica reaction: experimental study and numerical simulations, J. Mater. Civ. Eng. 18 (2006) 588–596.

[20] L.D. Glasser, N. Kataoka, On the role of calcium in the alkali-aggregate reaction, Cem. Concr. Res. 12 (1982) 321–331.

[21] F. Gaboriaud, A. Nonat, D. Chaumont, A. Craievich, Aggregation and gel formation in basic silico- calco- alkaline solutions studied: a SAXS, SANS, and ELS study, J. Phys. Chem. B 103 (1999) 5775–5781.

[22] S. Urhan, Alkali silica and pozzolanic reactions in concrete. Part 1: interpretation of published results and an hypothesis concerning the mechanism, Cem. Concr. Res. 17 (1987) 141–152.

[23] R.F. Bleszynski, M.D. Thomas, Microstructural studies of alkali-silica reaction in fly ash concrete immersed in alkaline solutions, Adv. Cem. Based Mater. 7 (1998) 66–78.

[24] S. Chatterji, The role of Ca(OH) in the breakdown of Portland cement concrete due to alkali-silica reaction, Cem. Concr. Res. 9 (1979) 185–188.

[25] T. Ichikawa, M. Miura, Modified model of alkali-silica reaction, Cem. Concr. Res. 37 (2007) 1291–1297.

[26] B.P. Gautam, D.K. Panesar, The effect of elevated conditioning temperature on the ASR expansion, cracking and properties of reactive spratt aggregate concrete, Constr. Build. Mater. 140 (2017) 310–320.

[27] J. Lindgård, Ö. Andiç-Çakr, I. Fernandes, T.F. Rønning, M.D. Thomas, Alkali–silica reactions (ASR): literature review on parameters influencing laboratory performance testing, Cem. Concr. Res. 42 (2012) 223–243.

[28] X. Qiu, J. Chen, G. Ye, G. De Schutter, A 3D reactive transport model for simulation of the chemical reaction process of ASR at microscale, Cem. Concr. Res. 151 (2022), 106640.

[29] H. Wang, J. Gillott, Mechanism of alkali-silica reaction and the significance of calcium hydroxide, Cem. Concr. Res. 21 (1991) 647–654.

[30] G.D. Guthrie, J.W. Carey, A thermodynamic and kinetic model for paste–aggregate interactions and the alkali–silica reaction, Cem. Concr. Res. 76 (2015) 107–120.

[31] J. Chen, G. Ye, A lattice boltzmann single component model for simulation of the autogenous self-healing caused by further hydration in cementitious material at mesoscale, Cem. Concr. Res. 123 (2019), 105782.

[32] X. Qiu, J. Chen, M. Deprez, V. Cnudde, G. Ye, G. De Schutter, 3D microstructure simulation of reactive aggregate in concrete from 2D images as the basis for ASR simulation, Materials 14 (2021).

[33] R. Mills, V.M. Lobo, Self-diffusion in Electrolyte Solutions: A Critical Examination of Data Compiled From the Literature, Elsevier, 2013.

[34] S. Girimaji, Lattice Boltzmann Method: Fundamentals and Engineering Applications With Computer Codes, 2013.

[35] Z. Chai, C. Huang, B. Shi, Z. Guo, A comparative study on the lattice boltzmann models for predicting effective diffusivity of porous media, Int. J. Heat Mass Transf. 98 (2016) 687–696.

[36] D. d'Humieres, Multiple–relaxation–time lattice boltzmann models in three dimensions, Philosophical Transactions of the Royal Society of London. Series A: Mathematical, Physical and Engineering Sciences 360 (2002) 437–451.

[37] P. Wijnen, T. Beelen, J. De Haan, C. Rummens, L. Van de Ven, R. Van Santen, Silica gel dissolution in aqueous alkali metal hydroxides studied by 29Si-NMR, J. Non-Cryst. Solids 109 (1989) 85–94.

[38] J. Visser, Fundamentals of alkali-silica gel formation and swelling: condensation under influence of dissolved salts, Cem. Concr. Res. 105 (2018) 18–30.

[39] T. Kim, J. Olek, H. Jeong, Alkali–silica reaction: kinetics of chemistry of pore solution and calcium hydroxide content in cementitious system, Cem. Concr. Res. 71 (2015) 36–45.

[40] Z.G. Shi, G.Q. Geng, A. Leemann, B. Lothenbach, Synthesis, characterization, and water uptake property of alkali-silica reaction products, Cem. Concr. Res. 121 (2019) 58–71.

[41] A. Leemann, B. Münch, The addition of caesium to concrete with alkali-silica reaction: implications on product identification and recognition of the reaction sequence, Cem. Concr. Res. 120 (2019) 27–35.

[42] A. Leemann, Z.G. Shi, J. Lindgård, Characterization of amorphous and crystalline ASR products formed in concrete aggregates, Cem. Concr. Res. 137 (2020), 106190.

[43] X. Hou, L.J. Struble, R.J. Kirkpatrick, Formation of ASR gel and the roles of CSH and portlandite, Cem. Concr. Res. 34 (2004) 1683–1696.

[44] B. Lothenbach, D.A. Kulik, T. Matschei, M. Balonis, L. Baquerizo, B. Dilnesa, G. D. Miron, R.J. Myers, Cemdata18: a chemical thermodynamic database for hydrated Portland cements and alkali-activated materials, Cem. Concr. Res. 115 (2019) 472–506.

[45] G.S. Grimmett, et al., Probability and Random Processes, Oxford university press, 2020.

[46] G. Geng, Z. Shi, A. Leemann, C. Borca, T. Huthwelker, K. Glazyrin, I.V. Pekov, S. Churakov, B. Lothenbach, R. Dähn, et al., Atomistic structure of alkali-silica reaction products refined from X-ray diffraction and micro X-ray absorption data, Cem. Concr. Res. 129 (2020), 105958.

[47] C. Dunant, Experimental and Modelling Study of the Alkali-silica-reaction in Concrete, Technical Report, EPFL, 2009.

[48] R. Helmuth, D. Stark, S. Diamond, M. Moranville-Regourd, Alkali-silica reactivity: an overview of research, Contract 100 (1993) 202.

[49] M. Mihara, R. Sasaki, Radio-nuclides Migration Datasets (RAMDA) on Cement, Bentonite and Rock for the Performance Assessment of TRU Waste Repository in Japan, Technical Report, Japan Nuclear Cycle Development Inst, 2005.

[50] L.D. Glasser, N. Kataoka, The chemistry of 'alkali-aggregate'reaction, Cem. Concr. Res. 11 (1981) 1–9.

[51] T. Kim, J. Olek, Chemical sequence and kinetics of alkali–silica reaction part ii. A thermodynamic model, J. Am. Ceram. Soc. 97 (2014) 2204–2212.

[52] M. Thomas, The effect of supplementary cementing materials on alkali-silica reaction: a review, Cem. Concr. Res. 41 (2011) 1224–1231.

[53] S.M. Shafaatian, A. Akhavan, H. Maraghechi, F. Rajabipour, How does fly ash mitigate alkali–silica reaction (ASR) in accelerated mortar bar test (ASTM C1567)? Cem. Concr. Compos. 37 (2013) 143–153.

[54] K. Andersson, B. Allard, M. Bengtsson, B. Magnusson, Chemical composition of cement pore solutions, Cem. Concr. Res. 19 (1989) 327–332.

[55] W. Hansen, Studies relating to the mechanism by which the alkali-aggregate reaction proceeds in concrete, J. Am. Concr. Inst. 15 (1944) 213–227. Cited By 51.

[56] C.S. Thomas, Toward a systematic understanding of party-group relations in liberal democracies, in: Political Parties and Interest Groups: Shaping Democratic Governance, Lynne Rienner, Boulder, CO, 2001, pp. 269–291.

[57] D. Bulteel, E. Garcia-Diaz, C. Vernet, H. Zanni, Alkali–silica reaction: a method to quantify the reaction degree, Cem. Concr. Res. 32 (2002) 1199–1206.

[58] S. Guo, Q.L. Dai, L. Chang, Y.H. Hu, X.F. Xie, R.Z. Si, J.Q. Wang, Kinetic analysis and thermodynamic simulation of alkali-silica reaction in cementitious materials, Journal of the American Ceramic Society 102 (2019) 1463–1478.

[59] E. Garcia-Diaz, J. Riche, D. Bulteel, C. Vernet, Mechanism of damage for the alkali–silica reaction, Cem. Concr. Res. 36 (2006) 395–400.

[60] J. Ponce, O. Batic, Different manifestations of the alkali-silica reaction in concrete according to the reaction kinetics of the reactive aggregate, Cem. Concr. Res. 36 (2006) 1148–1156.

[61] F. Rajabipour, H. Maraghechi, G. Fischer, Investigating the alkali-silica reaction of recycled glass aggregates in concrete materials, J. Mater. Civ. Eng. 22 (2010) 1201–1208.

[62] C.F. Dunant, K.L. Scrivener, Micro-mechanical modelling of alkali–silica-reaction-induced degradation using the amie framework, Cem. Concr. Res. 40 (2010) 517–525.

[63] T. Miura, S. Multon, Y. Kawabata, Influence of the distribution of expansive sites in aggregates on microscopic damage caused by alkali-silica reaction: insights into the mechanical origin of expansion, Cem. Concr. Res. 142 (2021), 106355.

[64] T. Ichikawa, Alkali–silica reaction, pessimum effects and pozzolanic effect, Cem. Concr. Res. 39 (2009) 716–726.

[65] I. Moundoungou, D. Bulteel, E. Garcia-Diaz, V. Thiéry, P. Dégrugilliers, J. Hammerschlag, Reduction of ASR expansion in concretes based on reactive chert aggregates: effect of alkali neutralisation capacity, Constr. Build. Mater. 54 (2014) 147–162.

[66] M. Shakoorioskooie, M. Griffa, A. Leemann, R. Zboray, P. Lura, Alkali-silica reaction products and cracks: X-ray micro-tomography-based analysis of their spatial-temporal evolution at a mesoscale, Cement and Concrete Research 150 (2021) 106593.

[67] G. Geng, Z. Shi, A. Leemann, K. Glazyrin, A. Kleppe, D. Daisenberger, S. Churakov, B. Lothenbach, E. Wieland, R. Dähn, Mechanical behavior and phase change of alkali-silica reaction products under hydrostatic compression, acta crystallographica section B: structural scienceCrystal Engineering and Materials 76 (2020).

[68] H. Maraghechi, F. Rajabipour, C.G. Pantano, W.D. Burgos, Effect of calcium on dissolution and precipitation reactions of amorphous silica at high alkalinity, Cem. Concr. Res. 87 (2016) 1–13.